

Combined influences of seasonal East Atlantic Pattern and North Atlantic Oscillation to excite Atlantic multidecadal variability in a climate model

Yohan Ruprich-Robert · Christophe Cassou

Received: 3 June 2013 / Accepted: 16 April 2014 / Published online: 27 May 2014
© Springer-Verlag Berlin Heidelberg 2014

Abstract The physical processes underlying the internal component of the Atlantic Multidecadal Variability (AMV) are investigated from a 1,000-yr pre-industrial control simulation of the CNRM-CM5 model. The low-frequency fluctuations of the Atlantic Meridional Overturning Circulation (AMOC) are shown to be the main precursor for the model AMV. The full life cycle of AMOC/AMV events relies on a complex time-evolving relationship with both North Atlantic Oscillation (NAO) and East Atlantic Pattern (EAP) that must be considered from a seasonal perspective in order to isolate their action; the ocean is responsible for setting the multidecadal timescale of the fluctuations. AMOC rise leading to a warm phase of AMV is statistically preceded by wintertime NAO+ and EAP+ from \sim Lag $-40/-20$ yrs. Associated wind stress anomalies induce an acceleration of the subpolar gyre (SPG) and enhanced northward transport of warm and saline subtropical water. Concurrent positive salinity anomalies occur in the Greenland–Iceland–Norwegian Seas in link to local sea-ice decline; those are advected by the Eastern Greenland Current to the Labrador Sea participating to the progressive densification of the SPG and the intensification of ocean deep convection leading to AMOC strengthening. From \sim Lag -10 yrs prior an AMOC maximum, opposite relationship is found with the NAO for both summer and winter seasons. Despite negative lags, NAO– at that time is consistent with the atmospheric response through teleconnection to the northward shift/intensification of the Inter Tropical Convergence Zone in link to the ongoing warming of tropical north Atlantic basin due to AMOC

rise/AMV build-up. NAO– acts as a positive feedback for the full development of the model AMV through surface fluxes but, at the same time, prepares its termination through negative retroaction on AMOC. Relationship between EAP+ and AMOC is also present in summer from \sim Lags $-30/+10$ yrs while winter EAP– is favored around the AMV peak. Based on additional atmospheric-forced experiments, both are interpreted as the local seasonal-dependent atmospheric response to warmer North Atlantic. Finally, advection of fresher water from the tropical basin created by local atmosphere/ocean anomalous circulation on one hand and from the Arctic on the other hand due to large-scale sea ice melting leads to decrease of density in the SPG and contributes terminating the model AMOC/AMV events. All together, the combined effects of NAO and EAP, their intertwined seasonal forcing/forced role upon/by the ocean and the primary role of salinity anomalies associated with oceanic dynamical changes acting as an integrator are responsible in CNRM-CM5 for an irregular and damped mode of variability for AMOC/AMV that takes about 35–40 (15–20) years to build up (dissipate).

Keywords Atlantic Multidecadal Variability (AMV) · Atlantic Meridional Overturning Circulation (AMOC) · North Atlantic Oscillation (NAO) · East Atlantic Pattern (EAP) · Ocean–atmosphere interactions · Internal climate variability

1 Introduction

Public understanding, perception and recognition of climate change due to human activities are greatly shadowed by internal variability that occurs over a wide range of time

Y. Ruprich-Robert (✉) · C. Cassou
Climate Modelling and Global Change Team, CERFACS/
CNRS, 42 Avenue Gaspard Coriolis, 31057 Toulouse, France
e-mail: ruprich@cerfacs.fr

scales (from days to several decades). Also referred to as “noise”, the latter intrinsically arises from the interactions between all the climate subsystems (atmosphere, ocean, cryosphere, continents and biosphere) that are characterized by different physical/dynamical/chemical properties. The internal variability is superimposed to the so-called externally forced variability that comprises natural (solar activity and volcanism) and anthropogenic sources (emissions of greenhouse gases—GHG, sulfate aerosols etc.). The weight of internal versus forced component increases from global to regional scale (Deser et al. 2012). The time of emergence (ToE) defined as the “date” from which the climate signals induced by anthropogenic forcings emerge from the noise is thus yet to come for most of the regions while it can be detected on planetary-integrated quantities (e.g. Hegerl et al. 2007). Estimated from models of the 3rd Coupled Model Intercomparison Project (CMIP3), the ToE is relatively near though (this decade or the next) for temperature related fields over a broad tropical band (except in the equatorial eastern Pacific) and at polar latitudes, but it could be delayed to 2030–2040 at midlatitudes or even later for some specific locations such as the North Atlantic basin and the Austral Ocean (Hawkins and Sutton 2012). Over there, it is thus essential to understand the origin of the internal modes, their dynamics and their evolution in order to disentangle their fingerprint from observed patterns and to assess their relative contribution for near future climate evolutions (from one-to-three decades).

IPV and AMV standing respectively for Inter-decadal Pacific Variability (Zhang et al. 1997) and Atlantic Multidecadal Variability, also referred to as Atlantic Multidecadal Oscillation (AMO) by many authors (e.g. Kerr 2000), are the two main modes of variability at decadal timescale whose weight can either aggravate or moderate, depending of their phase, the long-term warming trends caused by anthropogenic forcing (see for instance Meehl et al. 2009 for the accelerated global warming in the 1970s and 1980s and Meehl et al. 2011 for the ongoing “hiatus decade” in the 2000s, in link to IPV). AMV is defined as the low-pass filter (decadal timescale) sea surface temperature (SST) anomalies in the North Atlantic obtained after having removed the signal associated with the external forcings; estimation of the latter can be assessed through several techniques (e.g. Trenberth and Shea 2006; Ting et al. 2009, etc.). The AMV is characterized by a basin-scale anomalous pattern of same sign with maximum loading in the subpolar gyre (SPG) and eastern midlatitude basins (e.g. Schlesinger and Ramankutty 1994). Its precise preferential timescale of variability is difficult to assess due to the shortness of the observed period. A 60–100-year range covers most of the estimates in agreement with analyses from longer SST time series reconstructed from

proxies (e.g. Gray et al. 2004, using tree-rings going back to ~ 1600). Within this frequency band, the SST standard deviation averaged over the North Atlantic basin is equal to ~ 0.16 °C corresponding to about 35 % of the total variance estimated from yearly mean data. Through atmospheric teleconnection, AMV seems to control a large part of the decadal variability over the Atlantic surrounding continents, especially in summertime (Wang et al. 2012, among others). For a positive phase (basin-wide warmer North Atlantic), hurricane activity is clearly reinforced (e.g. Goldenberg et al. 2001; Vimont and Kossin 2007), summer precipitations over Western Europe and the Sahel are intensified (e.g. Sutton and Dong 2012; Mohino et al. 2011, respectively) while drought conditions prevail in the Nordeste Brazil (e.g. Folland et al. 2001) and in the Great Plains of the North American continent (e.g. Enfield et al. 2001; McCabe et al. 2004; Sutton and Hodson 2005).

The extraction of the AMV, as a strict internal mode of variability, and its weight in the total variance of the North Atlantic SST (defined as the 0° – 60° N average of annual mean SST anomalies, hereafter NASST), is not straightforward though from the sole observations. Based on model analyses from CMIP3 and the latest CMIP5 exercise, the low frequency observed NASST fluctuation over the last 150 years or so, indeed appears to be the final product of multiple factors (Terray 2012) combining external forcings together with internal dynamics, but the weight between factors is clearly model dependant. In Otterå et al. (2010) and Swingedouw et al. (2013), solar and volcanoes play a crucial role, while Chang et al. (2011) and more recently Booth et al. (2012) point out the dominant action of the anthropogenic sulfate aerosols. In the latter study based on the HadGEM model, external forcings control all together about half of the observed NASST variance, but this result is very controversial though because HadGEM appears unique amongst in the CMIP5 models in producing such a strong response to aerosols changes over the North Atlantic (Chiang et al. 2013; Zhang et al. 2013). Similarly, the importance of the volcanoes in Swingedouw et al. (2013) is debatable because of the presence of an overly dominant intrinsic decadal oscillatory mode of variability in the IPSL model that resonates with the timing of the late XXth century major eruptions. Therefore, there is still plenty of room for internal variability, i.e. AMV dynamics, to explain a large part of the observed NASST low frequency variability as convincingly shown in numerous studies based either on multi-model or ensemble experiments (see e.g. Knight 2009; Ting et al. 2009 respectively).

Additionally, DelSole et al. (2011) argues that a planetary pattern of multidecadal variability whose origin is purely internal and whose maximum loading is found in the

Atlantic, a.k.a. the AMV, even exists and is separable from the anthropogenic-forced response. The latter internal mode could have significantly contributed to the accelerating warming trend over 1977–2008 with respect to the previous decades of comparable radiative imbalance due to external forcings. Within this framework, the AMV is interpreted as a fingerprint of broader interhemispheric seesaw variability (Stocker 1998; Wang et al. 2012) supporting the hypotheses for a driving role of the Atlantic Meridional Overturning Circulation (AMOC, Wunsch 2002) variability. But observations are too sparse, often too poor in quality and limited to the surface ocean in most of regions to draw firm and robust conclusions from the sole available data. Understanding and evidences mostly rely on models of different complexities (from fully coupled Global Circulation Models—GCM to simpler configurations allowing for very long integration in time). When run with constant external forcings, the models confirm the contribution of natural internal dynamics to the genesis of AMV types of variability. In most of them, AMV is also found to lag AMOC fluctuations by a few years (e.g. Medhaug and Furevik 2011 and references therein) whatever the characteristics of the latter that could clearly differ among models as there is no consensus at all about the driving internal mechanisms. AMOC fluctuations have been shown to be associated with changes in poleward ocean heat and salt transport originated either from the southern hemisphere (e.g. Biastoch et al. 2008; Marini et al. 2011, Graham et al. 2011), the tropics (among others, Delworth and Mann 2000; Vellinga and Wu 2004; Mignot and Frankignoul 2005; Knight et al. 2005), the Arctic latitudes (e.g. Jungclaus et al. 2005; Hawkins and Sutton 2007) or a combination of all three. AMOC variability is though almost always accompanied by density fluctuations in the Nordic oceanic convection regions (Delworth et al. 1993; Marshall et al. 2001; Bentsen et al. 2004; Medhaug et al. 2011, among others). But the origins of those anomalies, their underlying mechanisms and their respective weight and interaction (freshwater versus momentum fluxes, advection versus local air–sea exchanges, sea ice role etc.), vary from one model to the next. AMOC fluctuations could thus be viewed either as a response to purely stochastic atmospheric forcing that would excite an internal mode of variability of the ocean set by the shape and bathymetry of the Atlantic basin (e.g. Delworth et al. 1993; Griffies and Tziperman 1995; Guemas and Salas-Melia 2008; Deshayes and Frankignoul 2008; Kwon and Frankignoul 2012), or as the result of active, albeit weak, ocean–atmosphere coupling with the North Atlantic Oscillation (NAO, e.g. Timmermann et al. 1998; Eden and Willebrand 2001; Danabasoglu 2008) or the East Atlantic Pattern (EAP, Msadek and Frankignoul 2009), and the Tropical Atlantic Inter Tropical Convergence Zone (ITCZ, Vellinga and Wu 2004).

Considering the driving role of AMOC, it is not surprising that large discrepancies between models therefore appear for the AMV pattern itself and its preferred time-scale as shown in Medhaug and Furevik (2011) from CMIP3. Besides AMOC, those discrepancies could be explained by the mean states and mean biases of the coupled models, their resolution (Hodson and Sutton 2012), the intrinsic level of internal variability at the ocean surface that is unique to each model and could differ by a factor of 3 in some regions (Hawkins and Sutton 2012), and by the presence of several mechanisms, all leading to AMV, but whose respective weight may differ between the models or could even be non-stationary in time within a given model (Kwon and Frankignoul 2012). Improving our understanding of the low-frequency climate variability of a given model could thus be considered as prerequisite or upstream study to interpret results from decadal hindcasts recently performed within CMIP5 (Meehl et al. 2009; Taylor et al. 2012).

The goal of this paper is thus to document the intrinsic characteristics of the AMV in CNRM-CM5 (Voldoire et al. 2013) in line with other similar papers recently published for CMIP5 models (e.g. Wouters et al. 2012). The paper is organized as follows: Sect. 2 briefly describes the model and its performance over the North Atlantic. The properties of the model AMV are presented in Sect. 3 followed by a detailed description of its relationship with the atmosphere in Sect. 4. The full life cycle of model AMV events is documented in Sect. 5 and 6 and the results are summarized and further discussed in Sect. 7.

2 CNRM-CM5 model description, configuration and mean state over the North Atlantic

2.1 Model components and configuration

The coupled GCM used in this study is the fifth version of the CNRM-CM suite of models jointly developed at Météo-France and Cerfacs (Centre Européen de Recherche et de Formation Avancée en Calcul Scientifique). The atmospheric component is ARPEGE-Climat-5.2 (Action de Recherche Petite Echelle Grande Echelle, Déqué et al. 1994) derived from the ARPEGE/IFS operational weather prediction model maintained by Météo-France and the European Centre for Medium-Range Weather Forecasts. The configuration used for CMIP5 and the present study employs a T127 triangular horizontal truncation. Diabatic fluxes and nonlinear terms are calculated on a Gaussian grid of about 1.4° latitude by 1.4° longitude. The vertical is discretized over 31 levels (26 levels in the troposphere) using a progressive vertical hybrid coordinate extending from the ground up to 10 hPa). The ocean model in

CNRM-CM5 is part of a model hierarchy based on the Nucleus for European Modeling of the Ocean (NEMO) core (Madec 2008). CNRM-CM5 employs the version 3.2 of the code run globally on the so-called ORCA triangular grid at 1° resolution on average. The vertical is discretized over 42 levels with 18 in the first 250-m depth (10 m for the first level). The sea ice model component is GELATOv5 (Salas y Mélia 2002) and is directly embedded in the ocean component using the same horizontal grid. Energy and water fluxes at the surface are computed within the SURFEX module that is embedded in ARPEGE and includes three surface schemes for natural land, inland water (lakes) and sea/ocean areas based on the ISBA model (Noilhan and Planton 1989). SURFEX also provides the simulated total runoff converted into river discharge by the TRIP model (Total Runoff Integrating Pathways, Oki and Sud 1998) and ultimately passed to the ocean on a daily basis ensuring the closure of the global hydrological cycle. Finally, the coupling between the different components is handled by the 3rd version of OASIS (Ocean Atmosphere Sea Ice Soil, Valcke 2013) on a 24-h basis. The model uses no flux correction: consistency between surfaces fluxes and transports is thus ensured but it allows the model for drifting to its own mean attractor with respect to reality. The reader is invited to refer to Voldoire et al. (2013) for a more complete documentation of the model.

2.2 Simulations

The AMV is investigated in the following from a 1,000-yr long integration of CNRM-CM5 where all the external forcings (solar irradiance, anthropogenic greenhouse gases, ozone, aerosols, etc.) are fixed to their estimated 1850 pre-industrial values. A volcanic background is applied along the integration that will be referred as to PiCTL following the CMIP5 nomenclature (Taylor et al. 2012). Initial conditions for PiCTL have been obtained from a 200-yr spin up run, then discarded in the subsequent analyses, starting from temperature and salinity 3-dimensional fields at rest from the 2005 World Ocean Atlas (WOA05, Locarnini et al. 2006; Antonov et al. 2006, respectively). The energy model is relatively well balanced at the ocean–atmosphere surface ($+0.38 \text{ W m}^{-2}$) leading to a very weak 3D temperature drift in the ocean ($+0.04 \text{ °C/century}$). By contrast, the CNRM-CM5 water flux is not conserved producing a spurious and significant drift in 3D salinity ($-0.011 \text{ psu/century}$), mainly due to erroneous and incompatible formulation in the concentration/dilution flux between NEMO and GELATO in the current version. Subarctic basins are the most affected with local values as high as $-0.043 \text{ psu/century}$ in the Greenland–Iceland–Norwegian (GIN) Seas. Note though that these values, even for salinity, are rather reasonable compared to the range from CMIP3 models

(Lucarini and Ragone 2011; Gupta et al. 2012). We verify that the artificial drifts do not introduce unsound behavior of the model such as catastrophic collapse of the AMOC, rapid and unrealistic sea-ice formation etc. In the following, all analyses will be applied to linearly detrended data over the full 1,000 years of integration.

2.3 Mean biases over the North Atlantic

The goal of this short section is not to provide an extensive documentation of the model performance but to present some of the mean flaws in the North Atlantic, our region of interest. The climatological SST and SSS (sea surface salinity) model minus observations (World Ocean Atlas 05 dataset) difference are presented in Fig. 1. The model is characterized by a pronounced cold bias off Newfoundland that contrasts to slightly anomalous warmer SST along the eastern coast of North America (shallow bathymetry region of Newfoundland bank and Gulf of Maine) and the western side of Greenland (Fig. 1a). CNRM-CM5 is also too cold in the tropics especially in the western basin dominated by a $\sim -1 \text{ °C}$ SST bias. The midlatitude “blue spot” in temperature is density compensated with waters that are too fresh along the $40^\circ\text{--}50^\circ$ latitudinal band extending eastward (Fig. 1b). These biases reach $6\text{--}7 \text{ °C}$ and $>3 \text{ psu}$ in SST and SSS respectively and lead *in fine* to spurious very strong stratification along the ocean column over the affected areas (mixed layer depth no deeper than 100 m at best). They directly reflect chronic ocean model deficiencies of the too-far north penetration of the Gulf Stream and the too-zonal North Atlantic Current (NAC) path compared to reality (Griffies et al. 2009 for CMIP3, Danabasoglu et al. 2014 for CMIP5). At such a low vertical and horizontal resolution, because of complex interactions between western boundary currents, bathymetry and the absence of resolved eddies, the SPG is southward shifted leading to enhanced transport of cold, fresh Labrador Sea water to the midlatitudes and to a southward displacement of the NAC. Mean barotropic stream function and mean upper 200-m currents (Fig. 1d, e) also reveal a clear eastward expansion of the SPG towards Europe by about $\sim 15^\circ$ and a confinement and consistent acceleration of the northward flow of the NAC within the $25^\circ\text{W}\text{--}15^\circ\text{W}$ longitudinal strip following the bathymetry constraint (see for instance Reverdin et al. 2003 for observational counterparts).

While most of these flaws are found in ocean models run in a forced mode using observed sea surface fields as above-mentioned, it is worth noting though that they are enhanced in a coupled context due to intrinsic biases of the atmosphere models. Errors in CNRM-CM5 for sea level pressure and low level wind at 850 hPa given in Fig. 1f are characterized by a southeastward (eastward) displacement of the mean Icelandic Low (Azores High) towards the

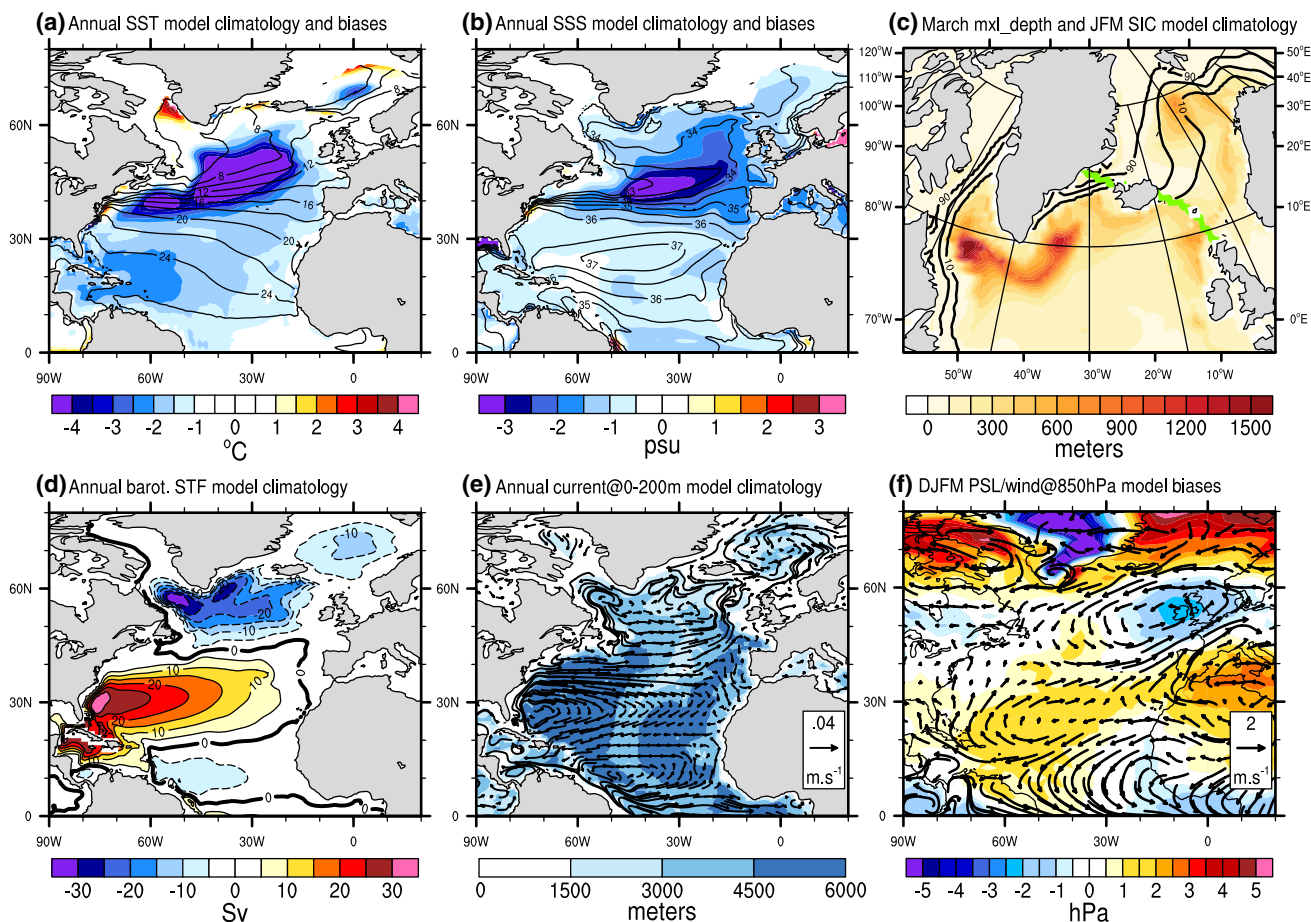


Fig. 1 **a** Climatological annual mean SST (contour) averaged over 1958–2002 from a CNRM-CM5 historical experiment and its difference with the World Ocean Atlas 05 dataset (*shading*). Sea ice areas are masked. **b** Same for SSS. **c** PiCTL model climatological mixed layer depth in March (*shading*) and mean sea ice concentration (in %, contour intervals are 40 % and start from 10 %). *Green line* corresponds to vertical transect used subsequently for assessing water exchanges between GIN Seas and the Northern Atlantic. **d** PiCTL

annual mean barotropic streamfunction with positive value meaning clockwise circulation. Contour intervals are 5 Sv. **e** PICTL mean ocean currents averaged over the upper 200 meters (vectors) superimposed on model bathymetry (*shading*). **f** Difference averaged over 1958–2002 from a CNRM-CM5 historical experiment and NCEP climatological December–March Sea Level Pressure (*shading*) and wind at 850 hPa (vectors)

British Isles (western Mediterranean basin) leading to stronger westerlies from Florida to Europe and easterly biases over a broad 55°N–75°N latitudinal band. Those biases are extremely similar to the ones found when ARPEGE is run in a forced mode using observed SSTs. The erroneous rotational atmospheric circulation located off Ireland thus further contributes to the eastward expansion of the SPG and precludes the NAC to move north-eastward from the central basin to Iceland as observed (e.g. Brambilla and Talley 2008), thus favoring the longer route along the European continental shelf (Hakkinen et al. 2011). The too-zonal atmospheric flow at midlatitudes also contributes to the southward displacement of the SPG and subtropical gyre (STG) latitudinal boundaries and to the 10°-wide extension of the Gulf Stream (in latitude between 30° and 40°N) (Fig. 1e). Only winter characteristics for

wind and sea level pressure (SLP) are shown for ARPEGE since the dynamics of that season mainly controls the mean circulation of the ocean.

Despite the above-mentioned flaws in geographical positions, the CNRM-CM5 mean ocean dynamics and the deep convection zones are broadly consistent with the observations. SPG and STG have a maximum strength of –36 and 40 Sv respectively, which lies within the observational estimates for both (e.g. Hakkinen and Rhines 2004; Meinen et al. 2010, respectively). North Atlantic deep-water (NADW) formation as indicated by deep mixed layer depths (Fig. 1c), mostly occurs in PiCTL in the Labrador Sea (>1,500 m) and in the northern fringe of the SPG (~1,200 m in the Irminger Sea, ~600 m elsewhere). A secondary site is found in the GIN Seas with values as high as 800 m. The location of the maximum deep convection

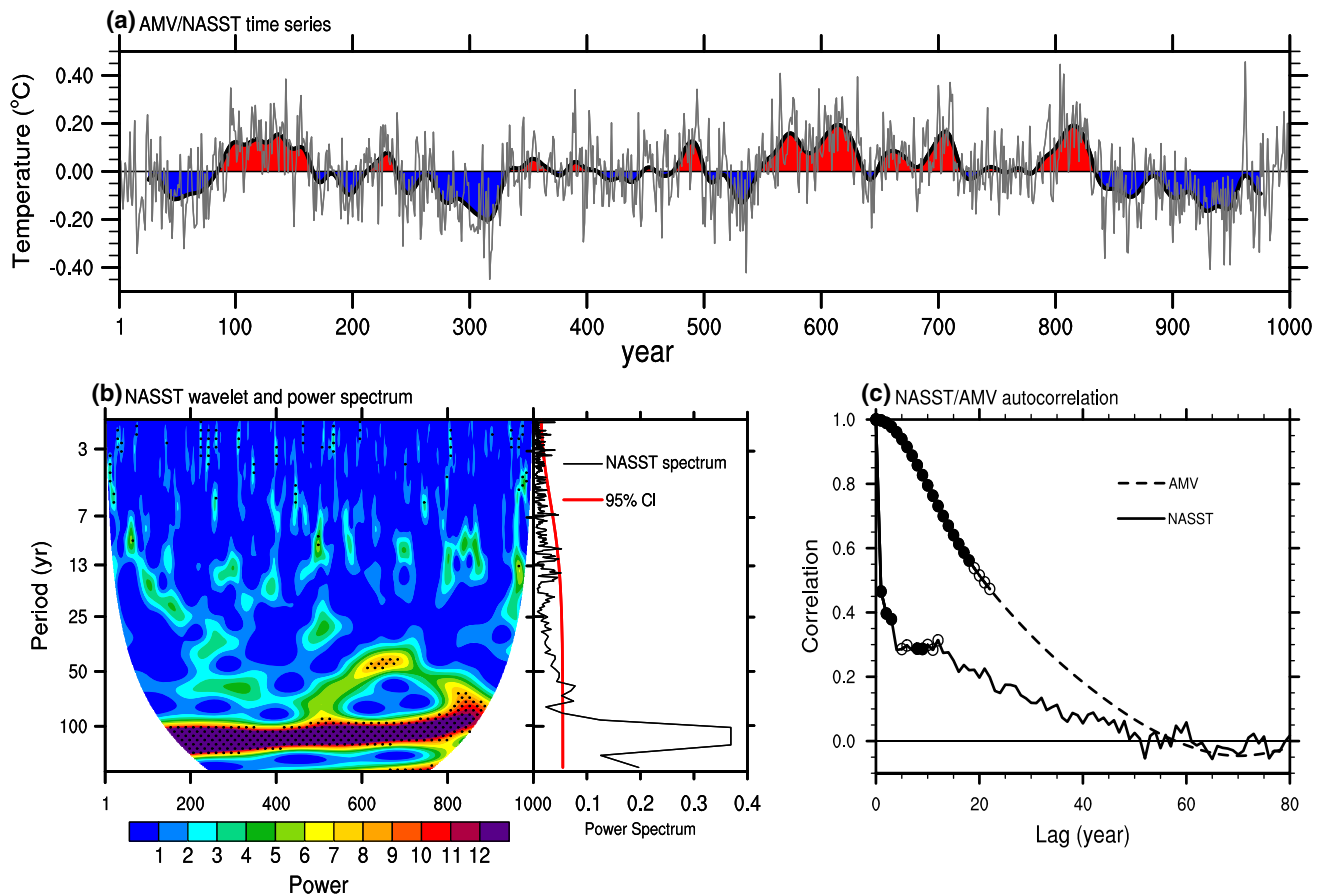


Fig. 2 **a** Annual NASST index computed as the grid area weighted averaged SST anomalies over 0° – 60° N in the Atlantic (*gray* time series) superimposed on the AMV index defined as the low-pass filtered NASST index using a Lanczos filter (51 weights and a 25-yr cutoff period, thick time series). **b** NASST wavelet and power

spectrum/significance following Torrence and Compo (1998). **c** Auto-correlation of NASST (*solid*) and AMV (*dashed*) indices. Significance at the 95 % (90 %) confidence level based on bootstrapping method (following Davison and Hinkley 1997) is given by *plain* (circles) *dots*

zones compare relatively well with the observational estimates (de Boyer Montégut et al. 2004). Most of the discrepancies occur along the Iceland-Bay of Biscay arching pattern where mixing depths are clearly underestimated. This is again related to the climatological southward shift of the mean storm tracks in coherence with the pressure centers of actions displaced to the east in the model (Fig. 1f). The March sea-ice mean climatology is well captured especially in the Labrador Sea (Fig. 1c). Slight overestimation is found in the Greenland Sea where ice invades the northern coast of Iceland and episodically covers part of the GIN Seas (see the 10 % contour line).

3 Characteristics of the Atlantic Multidecadal Variability in CNRM-CM5

The North Atlantic Ocean variability in CNRM-CM5 is first assessed from the classical NASST index (Fig. 2a). Year-to-year fluctuations are superimposed on low-frequency

fluctuations characterized by the alternation of multidecadal, even centennial, pronounced cold and warm phases of different durations. A wavelet analysis (Torrence and Compo 1998) confirms that maximum energy is found within the 80–120-year band along the entire 1,000-yr integration (Fig. 2b). NASST spectrum accordingly shows that multidecadal-to-centennial periods clearly dominate the North Atlantic variability. Secondary and marginal power concentration tested against a red-noise process occurs at decadal time scale within the 10–15-year frequency band but the latter is intermittent. Minimum of energy is found around 25 years chosen as cutoff frequency for low-pass filtering (Lanczos filter, Duchon 1979) applied in the following to isolate the low-frequency behavior of CNRM-CM5, hereafter referred to as AMV for simplicity (Fig. 2a). The ratio of variance between the low-pass filtered (AMV index) and raw NASST index whose deviation standard is equal to 0.14°C , is about 40 %. Despite a significant strong power peak at centennial timescale in a Fourier perspective, it is important to note that neither AMV, nor even NASST, have oscillatory

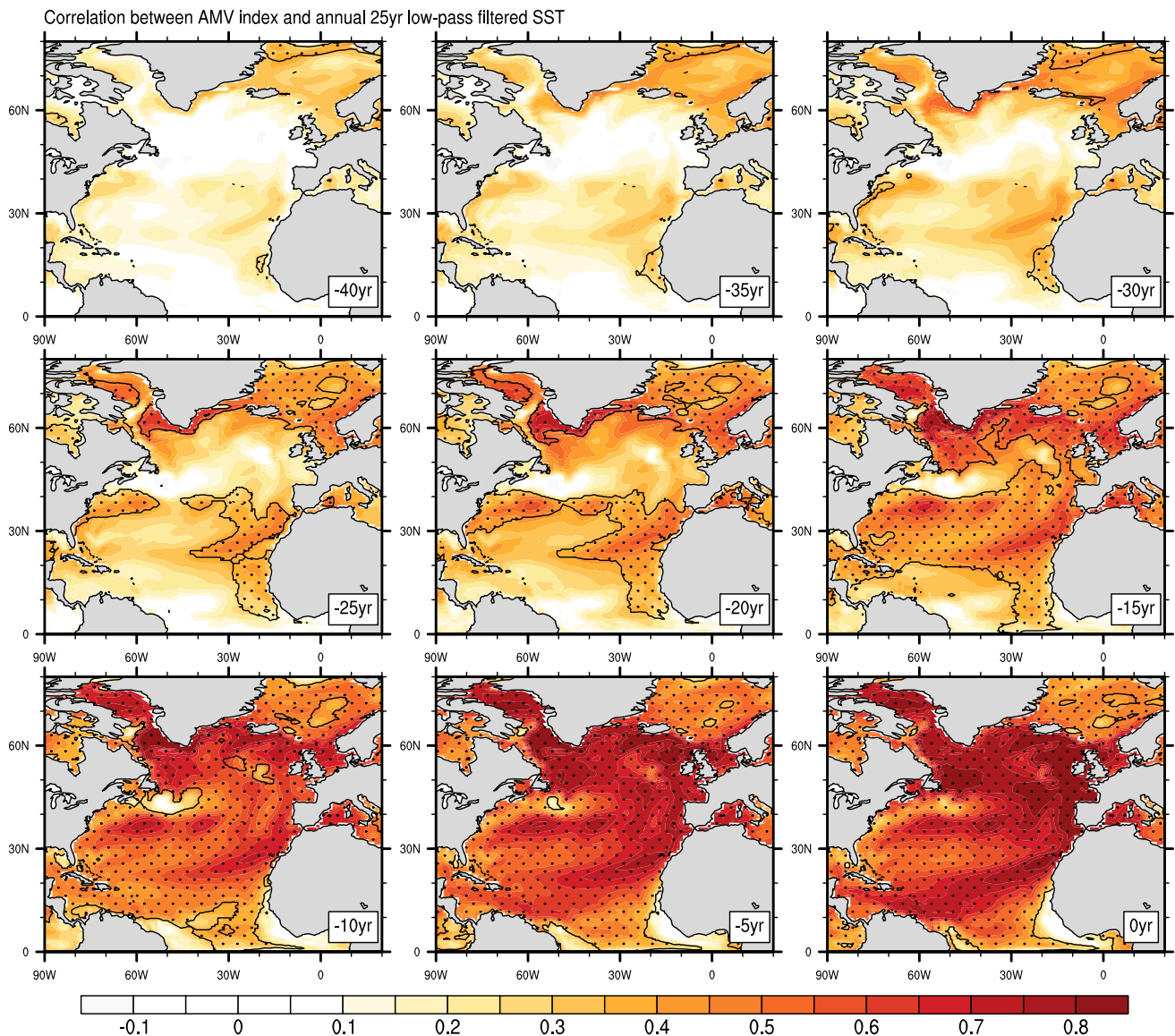


Fig. 3 Lagged correlation maps between AMV index and annual 25-yr low pass filtered SST. Lags are provided in the *lower-right corner* (negative values mean that AMV lags) and stippling stands for significance based on bootstrapping at the 95 % confidence level

characteristics as revealed by the autocorrelation of the indices (Fig. 2c) and confirmed by a Singular Spectrum Analysis (not shown). By construction, significance is rapidly lost for NASST (up to 12 years at the very most) compared to AMV (up to 20 years).

Lagged correlation maps for SST are given in Fig. 3 to follow the emergence of the model AMV. Correlation is preferred here to traditional regression to stress out the importance of the tropics in the full development of the AMV in CNRM-CM5. Because of lower variance compared to midlatitudes, tropical anomalies are indeed often masked out while their role can be crucial, as discussed later, even if their amplitudes are in the order of a tenth of degree. Significant warming starts along the sea-ice edge

between Greenland and Spitsbergen about 40-yr prior to maximum AMV (Lag -40 yr, Fig. 3 top left). Positive SST anomalies slowly invade the entire GIN Seas and propagate along the Eastern Greenland Current (EGC) towards the Labrador Sea (Lag -25 yr). Concomitant warming starts in the eastern side of the tropical basin and along the Gulf Stream. At Lag -15 yr, the western side and the northern fringe of the SPG have warmed significantly as well as the midlatitude/subtropics within a broad 15°N–40°N latitudinal band. Non-significant values are found in areas of erroneous overall stratification (between 45°N and 55°N, see previous section) and may suggest some impacts of the mean state/biases of the model in the setup of its AMV. From Lag -10 yr onwards, warming

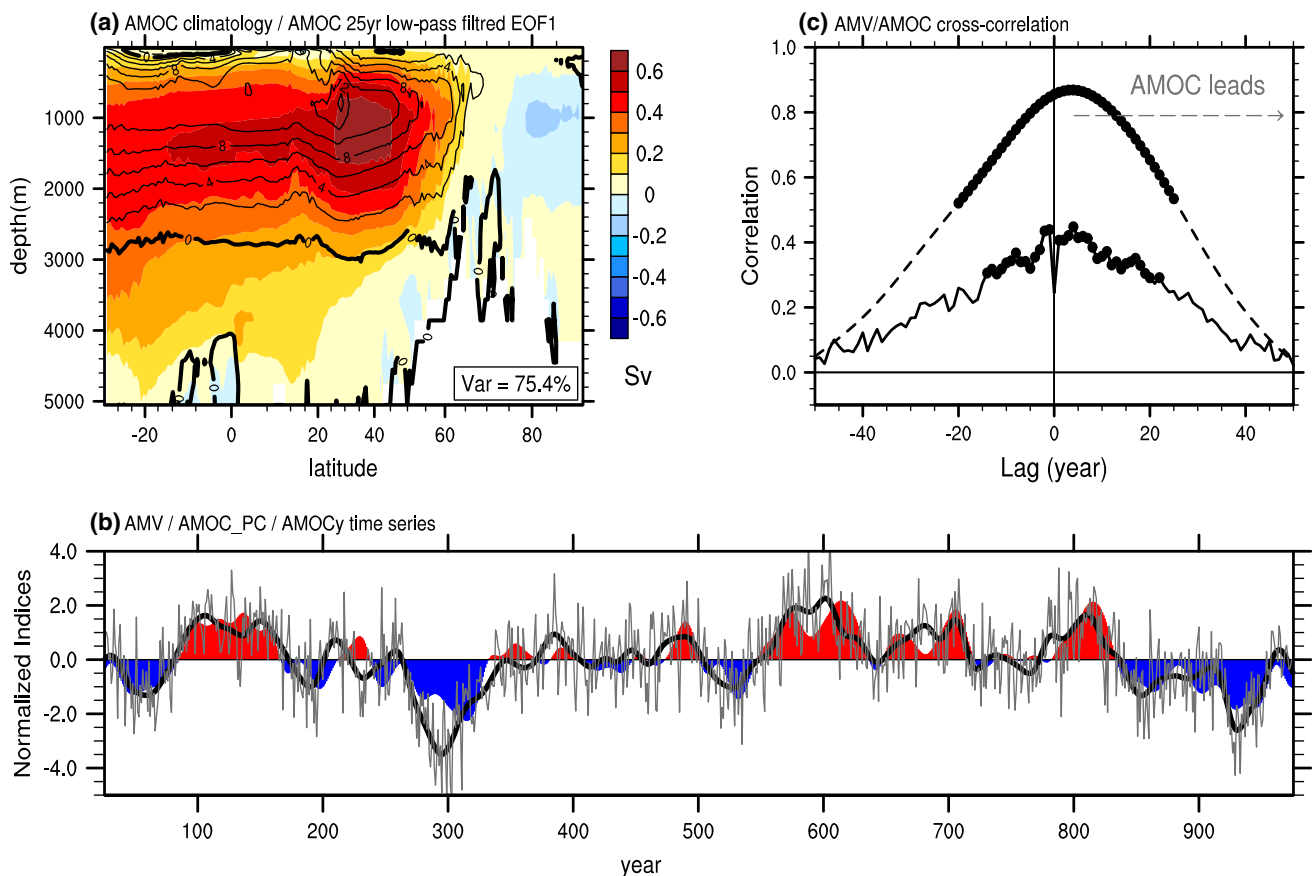


Fig. 4 **a** Climatological streamfunction of the annual mean zonally-integrated volume transport in the Atlantic (AMOC, contour interval is 2 Sv) superimposed on EOF1 pattern of the 25-yr low pass filtered AMOC (shading) explaining 75.4 % of the latter total variance. **b** Normalized PC (AMOC_PC, thick line) and AMOCy time series

(thin gray line) superimposed on the AMV index (blue/red filling). **c** Cross-correlation between AMV/NASST and AMOC_PC (dashed)/AMOCy (solid) indices. Significance at the 95 % confidence level based on bootstrapping method is given by plain dots

expands over the entire SPG domain and further penetrates southward in the tropics. When AMV peaks, the entire basin is warm with maximum loading (correlation >0.7) over the SPG region, along the European Coast and a band extending from the Canaries Isles to the Caribbean.

Consistently with DelSole et al. (2011)'s findings, regressed low-pass filtered 2-m temperature (T2M) onto the AMV index displays, in phase, a clear planetary pattern (not shown) that controls a large fraction of the global mean temperature low-frequency changes in CNRM-CM5 (correlation equal to 0.71 between AMV and global averaged T2M indices). The northern hemisphere warming linked to the AMV is interpreted as the surface fingerprint of changes in AMOC strength as suggested in several studies (see Knight et al. 2005; Zhang 2007 among others). Traditionally assessed by the meridional overturning mass streamfunction, the mean AMOC in CNRM-CM5 shows a classical clockwise cell that materializes the northward mass transport in the upper ocean up to about 60° of latitude where downwelling occurs (Fig. 4a) and NADW forms. Return flows

take place below $\sim 1,200$ m in the model and a maximum value equal to ~ 14 Sv ($1 \text{ Sv} = 10^6 \text{ m}^3 \text{ s}^{-1}$) is found around 800 m at 27°N . That climatological strength lies in the lower range of the 13–24 Sv observational estimates (Medhaug and Furevik 2011) from hydrographic data (e.g. Ganachaud and Wunsch 2000; Wunsch 2002), from the dedicated RAPID array at 26.5°N (Cunningham et al. 2007) or from satellite altimeter and Argo profiling float measurements (Willis 2010). The deeper anticlockwise overturning cell of Antarctic Bottom Water (AABW) is almost absent in CNRM-CM5 due to strong warm bias in the Austral Oceans that inhibits any deep-water formation there (Voldoire et al. 2013).

Since we seek for mechanisms at multidecadal timescale in link to AMV, AMOC variability is assessed in the following from empirical orthogonal function (EOF) applied on low pass filtered meridionally-averaged mass streamfunction. The leading mode displayed in Fig. 4a captures ~ 75 % of the low-frequency variance and projects very well onto the time-mean structure of the AMOC suggestive

of changes of its full body. Greater loading is found in the North Atlantic though (from 20°N to 50°N) and goes deeper with a maximum value equal to 0.6 Sv around $\sim 1,100$ m for a fluctuation of one standard deviation of the principal component (PC). The latter, hereafter referred to AMOC_PC index for simplicity, displays multidecadal to centennial fluctuations that closely resemble the AMV ones (Fig. 4b). No oscillatory behaviors are noted for AMOC_PC as for AMV but a strong cross correlation is found between the two indices with a maximum value of 0.91 when AMOC_PC leads AMV by about ~ 5 years (Fig. 4c). AMOC low frequency variability can be interpreted here as the overly dominant precursor of the AMV (linked to about 80 % of its variance).

Focus will be devoted in the following to the origins of the AMOC changes leading *in fine* to AMV. To do so, AMOC_PC is complemented by a new index called AMOCy, following Msadek and Frankignoul (2009)'s recommendation when the goal is to isolate the lead-lag relationships between the oceanic low-frequency fluctuations and the atmosphere that is dominated by very high frequency variability. AMOCy consists in projecting the raw annual mass streamfunction maps onto the low-frequency EOF pattern of AMOC given in Fig. 4a. By construction, AMOCy thus shares the same low-frequency variance as AMOC_PC but modulated by interannual changes on top of it (Fig. 4b). The rationale for this index relies on the fact that raw interannual patterns of AMOC variability mainly represents the wind-driven ocean response in the depth-meridional plane associated with El Niño Southern Oscillation (ENSO) and the NAO (Vellinga and Wu 2004), but not the full spin-up/spin-down of the NADW cell at the core of multidecadal changes. On a statistical point of view, significance for ocean–atmosphere lead-lag relationships is also better assessed because the time evolution of the AMOCy index is not affected by any temporal filtering applied a posteriori to isolate low-frequency characteristics; the filtering is instead a priori accounted in the spatial pattern itself. Thus lead-lag correlations between AMOCy and NASST indices (Fig. 4c) confirm that the AMV-AMOC ~ 5 yr lagged relationship (AMOC in advance) presented earlier in this section is not statistically perturbed by the 25-yr low-pass filter. Loss of correlation at lag 0 confirms that there is no in phase relationship between the annual North Atlantic SST and the AMOC low frequency variability.

4 Role of the atmosphere in the CNRM-CM5 AMOC/AMV multidecadal variability

Atmospheric variability is first assessed through decomposition in EOF conducted separately on winter

(December–March, DJFM) and summer (June–September, JJAS) seasonal averaged SLP over the North Atlantic–Europe domain (NAE, 20°N–80°N/90°W–30°E). We show in the following that stratifying into season, as opposed to use annual means, is crucial to understand the ocean–atmosphere interaction. Annual quantities are generally misleading because they mix forcing/response roles of the atmosphere upon/to the ocean that could be seasonal-dependant.

The leading wintertime EOF mode captures the NAO characterized by a seesaw structure between the Icelandic Low and the Azores High (Fig. 5a). When positive (negative), both centers of action are reinforced (slackened) leading to enhanced (diminished) westerlies at midlatitudes and trade winds in the subtropics (see Hurrell et al. 2003 for a complete review). In CNRM-CM5, the NAO represents a bit more than 40 % of the SLP NAE variance. The second mode (Fig. 5b) corresponds to the so-called East Atlantic Pattern (EAP, following Barnston and Livezey 1987's nomenclature) and represents about 15 % of the variance. The positive phase is characterized by a low-pressure monopole located off the British Island. The spatial patterns and the weights for both the NAO and the EAP match relatively well the observed ones but for a slight northeastward shift of the pressure poles in link to the mean biases of the midlatitude circulation that is too zonal in the model (see Sect. 2.3). Summertime NAO and EAP modes (contour, Fig. 5a, b) bear a strong resemblance to their wintertime counterparts provided a shift of the anomalous pressure centers. Note that amplitudes in summer are considerably reduced in consistence with the seasonal cycle of the variance of the extratropical atmospheric circulation.

The relationships between NAE atmospheric variability and AMOC low-frequency variability are investigated in the following through lead-lag correlations diagnostics. Maximum values are found between AMOCy and winter NAO+ when the latter leads by about 35 years [(-45/-25)-yr window, Fig. 5c]. Sign reversal in the winter NAO/AMOCy link occurs around 10-yr prior an AMOC maximum and NAO- persists onwards while significance is weak. Recall that there is no a posteriori filtering in AMOCy time series and in-phase relationship (isolated peak at lag 0) thus mostly reflects the fast response of the ocean to the interannual atmospheric forcing (Msadek and Frankignoul 2009). Earliest significant correlations are also found with winter EAP+ over the (-40/-30)-yr window prior an AMOC maximum (Fig. 5d). This link is lost between -30 yr and about -5 yr before the emergence of opposite sign correlation, i.e. with winter EAP- for Lag -5/+10 years. A clear signal pops out for the summertime EAP+ (Fig. 5d) that is favored in a very persistent way from ~ -30 to +10 years. Results are less striking for the

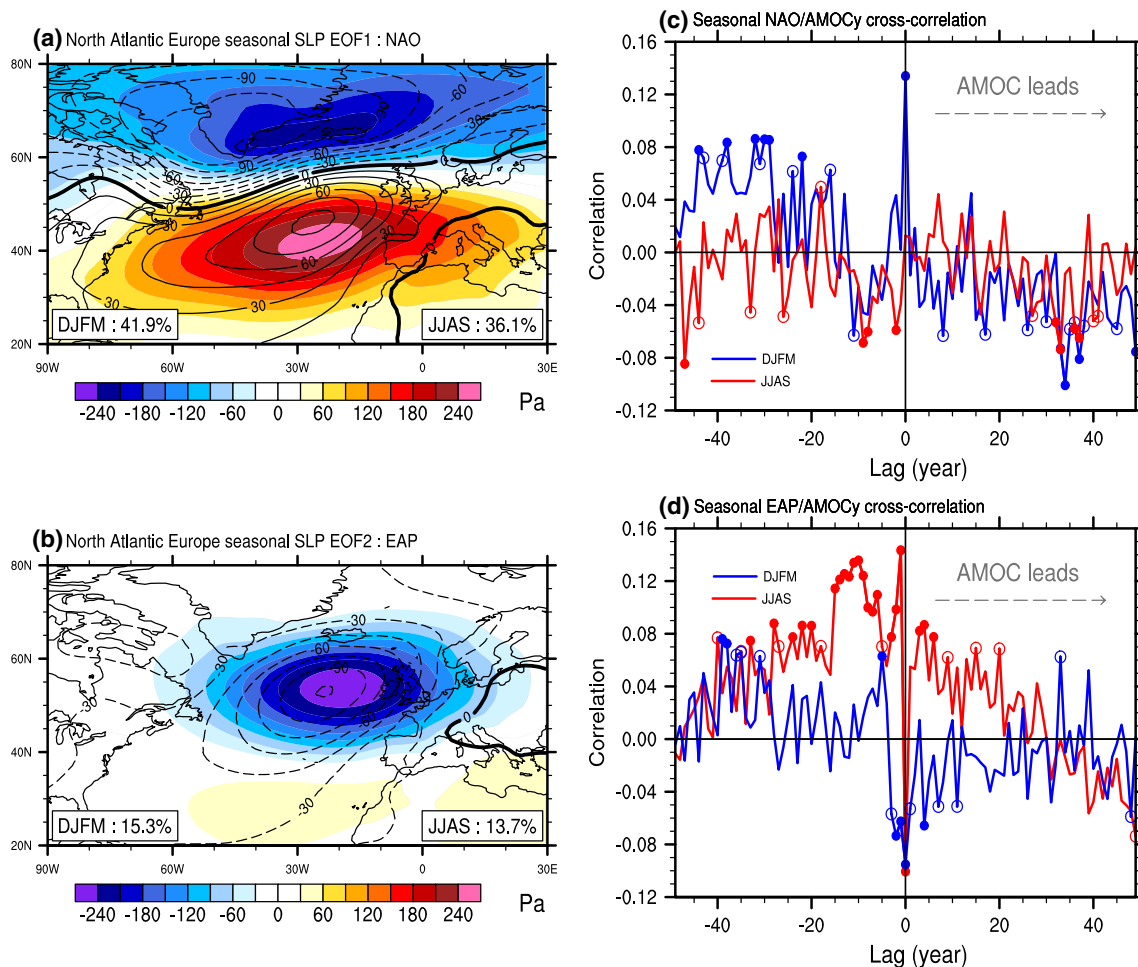


Fig. 5 **a** First and **b** second EOF maps of December–March (shading) and June–September (contour) mean sea level pressure in Pa. Percentages of explained variance are given in the lower corners. Contour interval is divided by two for summer. **c**, **d** Lead-lag

correlations between EOF PCs and AMOCy for winter (blue) and summer (red) seasons. Significance at the 95 % (90 %) confidence level based on bootstrapping method is given by plain dots (circles). Positive lags mean AMOC is leading

summertime NAO (Fig. 5c); significant correlation is obtained with NAO– over the (–10/0)-yr window and marginally later on around +35 yr in phase with wintertime NAO–.

Beside the fact that, by construction, correlation values based on unfiltered data (Fig. 5) are smaller as opposed to more traditional analyses where low-frequency filtering is applied, those are weak and without clear oscillatory behavior. This suggests that the CNRM-CM5 multidecadal variability of AMOC could be interpreted as the ocean integration of NAE atmospheric forcings without clear evidence for strong enough coupling or feedback to sustain oscillations. This interpretation would be consistent with the above-documented aperiodical properties of the AMOC variability and accordingly AMV that is mainly treated here as a byproduct of the latter. We verify that the two SLP modes have a white noise type of variability (not shown). Considering the persistent significant values over

several decades between AMOCy and NAO/EAP, the multidecadal AMOC in CNRM-CM5 seems to be driven by the low-frequency portion of the spectrum of atmospheric forcing similarly, for instance, to Delworth and Greatbatch (2000) and Dong and Sutton (2005) findings for the GFDL and the HadCM3 models respectively. Those studies report the critical role of the NAO to speed up the low-frequency variations of the AMOC. In our case, we show that EAP should be also included as a forcing in addition to the NAO in agreement with fewer papers such as Msadek and Frankignoul (2009). Earliest significances are found indeed for both modes in winter consistently with Krahnemann et al. (2001) who highlights that the latter season, with respect to summer, is responsible for most of the ocean forcing.

From a strict statistical point of view, negative lags indicate that the atmosphere is driving the AMOC. It is thus puzzling to note that the NAO/AMOCy relationship

switches sign while lags stay negative suggesting, at first glance, that both NAO+ and NAO− act as a forcing for AMOC as a function of lags. In a linear framework like in lead-lag correlations presented here, such an interpretation is misleading. Because of the multidecadal timescale characteristics of the CNRM-CM5 AMOC as documented from Fig. 2, short negative lags could capture to some extent the ocean influence upon the atmosphere while AMOC/AMV is still building up in response to earlier atmospheric forcing and associated low-frequency ocean adjustment. This calls for a detailed analysis of the full sequence and related mechanisms of a typical AMOC event in CNRM-CM5. Early stage [(-40/-20)-yr window] prior to an AMOC maximum where winter forcing dominates and late stage [(-20/+5)-yr] where forcing and response may intertwine are inspected separately in the next two sections.

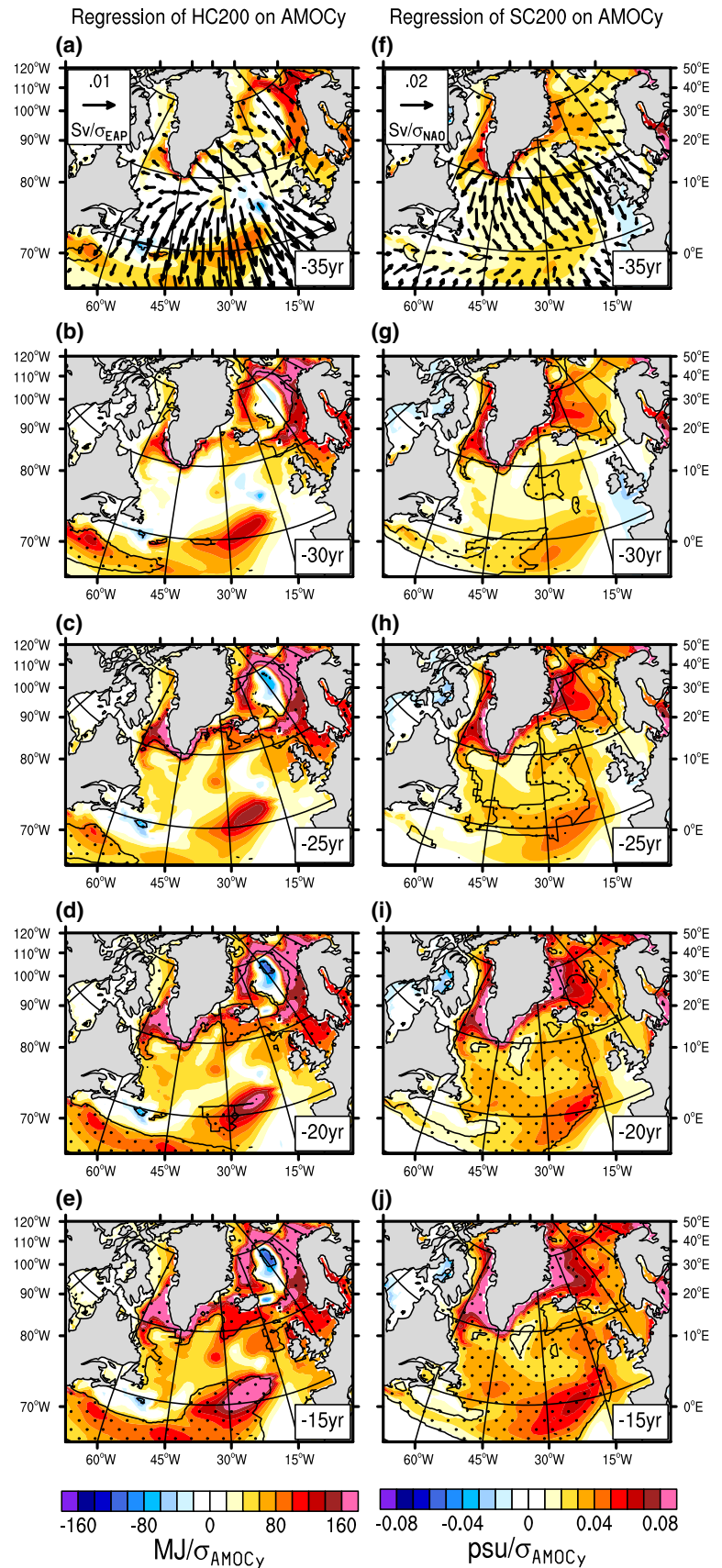
5 Early stage of the CNRM-CM5 AMV build-up

About 35 years prior to an AMOC maximum in response to atmospheric stochastic variability, the annual heat content of the upper ocean integrated from 0 to 200 m (hereafter referred to as HC200) starts rising along a broad 35°–45°N latitudinal band as well as in the GIN Seas with maximum loading on the eastern side of the cyclonic mean circulation (Fig. 6a). Mean salinity averaged over the upper 200 meter (hereafter SC200) also increases at midlatitudes and on the northern fringe of the SPG (Fig. 6f). In GIN by contrast to HC200, maximum anomaly is found on the western side of the gyre. Amplification clearly occurs from Lag -30 yr (Fig. 6b, g) and values get progressively more and more significant with time. These anomalous patterns are very much consistent with the ocean response to forcings from both NAO+ and EAP+ shown to be active in winter over the (-40/-25)-yr window. Anomalous momentum input from changes in the wind stress fields cause significant changes in the oceanic heat transport and its divergence. Much of this effect is due to changes in the Ekman transport (Fig. 6f) leading during NAO+ to anomalous convergence (i.e. downwelling) along 40°N and enhanced HC200 and SC200. NAO+ anomalous Ekman response is also associated with coastal upwelling along Greenland, which brings warmer and saltier water from subsurface to surface. Once generated, the heat and salt anomalies are advected by the mean current. NAO+ anomalous barotropic circulation is also characterized by a tripolar pattern consistent with a northward shift of the gyre (the intergyre-gyre, Marshall et al. 2001) leading to a westward contraction of the SPG and an acceleration of the NAC along the 35–45° latitudinal band (Fig. 7a). EAP+ leads also to an acceleration of the SPG, especially on its eastern side,

together with the intensification of the STG (Fig. 7c) in agreement with Hakkinen et al. (2011) and Barrier et al. (2013) from observations and idealized simulations, respectively. The NAC, and in particular its northward branch between 30°W and 15°W from the Azores to Iceland is enhanced in resonance with the climatological background (Fig. 1e). All together, the ocean adjustment to both NAO+ and EAP+ thus leads to enhanced northward advection of warm and saline water, which progressively invades the entire SPG, which is strengthening (Fig. 8a). This is particularly visible from SC200 where significance starts in the inner-rim of SPG at Lag -25 yr (Fig. 6h) with intensifying anomalies that propagate northwestward along the mean ocean circulation from the East (Fig. 6h–j). While salt accumulates in the center of the gyre through lateral advection (Born and Mignot 2012), it acts as a positive retroaction upon the SPG circulation following the so-called internal salinity feedback (hereafter S-feedback following Levermann and Born 2007). Density increases enough to cause stronger convection in the Labrador Sea from Lag -30-yr (Fig. 8a).

In CNRM-CM5, an additional and faster source of salt for the western side of SPG is found at the Denmark Strait (DS hereafter) and is also hypothesized to accelerate the Labrador Sea response. Though anomalous Ekman transport due to altered wind stress during EAP+ (Fig. 6a), volume inflow from the Atlantic to GIN Seas is intensified at the Iceland-Scotland Ridge (ISR). This leads to increased heat inflow as inferred from Fig. 9b from the model ISR transect (estimated from the PAGO tool, Deshayes et al. 2014) where positive temperature anomalies extend down to ~500 m. Anomalous heat is progressively advected along the Norwegian coast until Spitsbergen (Fig. 6a, c, e). Enhanced cyclonic gyre circulation in GIN in response to NAO+ (Fig. 7a) additionally contributes to the efficiency of the transport along Scandinavia. Note also that reinforced southerly winds during NAO+ and EAP+ produces an additional source of local warming through anomalous surface fluxes (Fig. 7b, d). All together, these factors inhibit the sea-ice formation as diagnosed from lead-lag correlations between model ice concentration leading EOF and AMOC (Fig. 10). Evidence for ice decline starts from ~30 yr prior to an AMOC maximum in both summertime and wintertime. In CNRM-CM5, the resulting effect is dominated by enhanced evaporation over ice-free zones leading in turn to increased surface salinity as shown in Fig. 6f, g. We verify based on a salinity budget that the changes in salinity content in GIN during AMOC rise are controlled not by the salt convergence term but by the surface water flux as revealed by significant correlation between AMOC and the latter term prior an AMOC maximum (Fig. 11a). The convergence term is only significant at positive lags, during AMOC declines. Enhanced

Fig. 6 5-yr running mean lagged-regression maps of annual ocean heat (left panels) and salt (right panels) content averaged over the upper 200 m on the 5-yr running averaged AMOCy index. Negative lags provided in the lower-right corner mean AMOCy is lagging and stippling stands for significance based on bootstrapping at the 95 % confidence level. Regressed Ekman transport on winter EAP and NAO is superimposed in a, f, respectively



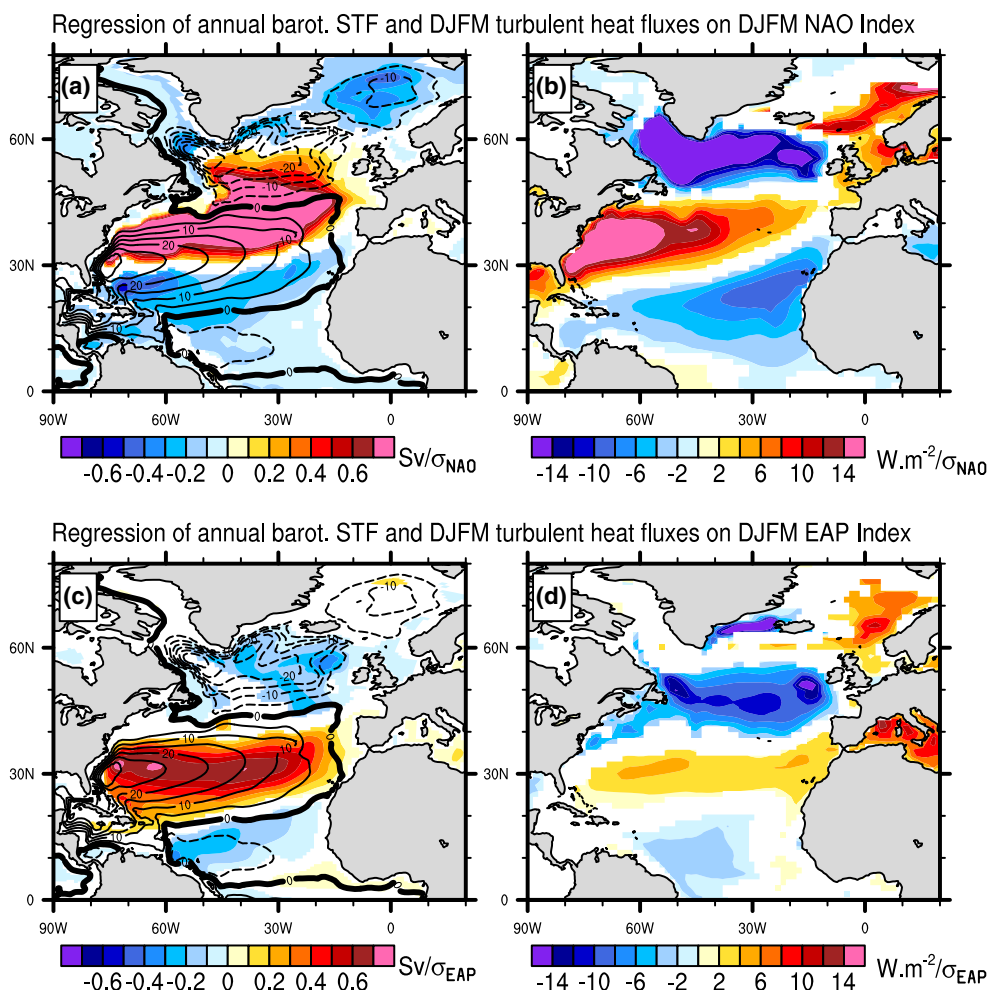


Fig. 7 Regression maps of annual barotropic streamfunction (*left panels*) and DJFM turbulent heat flux (*right panels*) on the DJFM NAO (**a, b**) and EAP (**c, d**) indices. Units are Sv and $W.m^{-2}$ per

standard deviation of PCs, respectively and non-significant points at the 95 % confidence level based on bootstrapping method are masked. Mean annual barotropic streamfunction is superimposed in **a, c**

evaporation appears in the GIN Seas -30 yr before an AMOC maximum (Fig. 11b), matching the sea-ice cover reduction from Iceland to Spitsbergen as well as along the Greenland coast. Figure 11c shows the annual evaporation regressed upon freshwater surface fluxes averaged over the GIN Seas domain. Enhanced evaporation again matches pretty well the sea-ice limit. All together, this confirms that surface fluxes and especially evaporation are mostly responsible for changes in salt content in GIN Seas.

The salinity excess is then advected by the East Greenland Current through DS towards the sinking regions in the Labrador basin, as revealed from the DS transect in Fig. 9c; it contributes to the intensification of the deep convection there in addition to salt inflow that progressively arrives along the SPG from its southeastern border as above documented. Thus, in CNRM-CM5, the GIN Seas may act as a convertor transforming heat anomalies from surface fluxes and inflow into salt anomalies in outflow. Indeed, marginal

significant temperature anomalies solely appear in DS at intermediate level (around 100-m depth, Fig. 9a) while they are very strong and extent deepward at the ISR inflow (Fig. 9b). In fact, surface warmer water along DS close to Iceland, albeit non significant, is associated with a recirculation current flowing to the North that is disconnected to the EGC (Fig. 1e and see for instance Nilsen et al. 2003, their Fig. 1 for observations). Concurrently, there is no salinity anomaly at ISR except at the surface between Iceland and Faroe (Fig. 9d) while they are pronounced at DS (Fig. 9c). The ISR surface salt excess comes, on one hand from the advection of the Greenland-side anomalies that recirculate along the climatological gyre in the GIN Seas (Figs. 1d, e and 6g-i), and on the other hand from the response through evaporation to local sea-ice decline; it is not associated with the inflow of Atlantic water.

The chain of events presented so far and displayed in Fig. 6 is much easier to follow on SC200 than HC200,

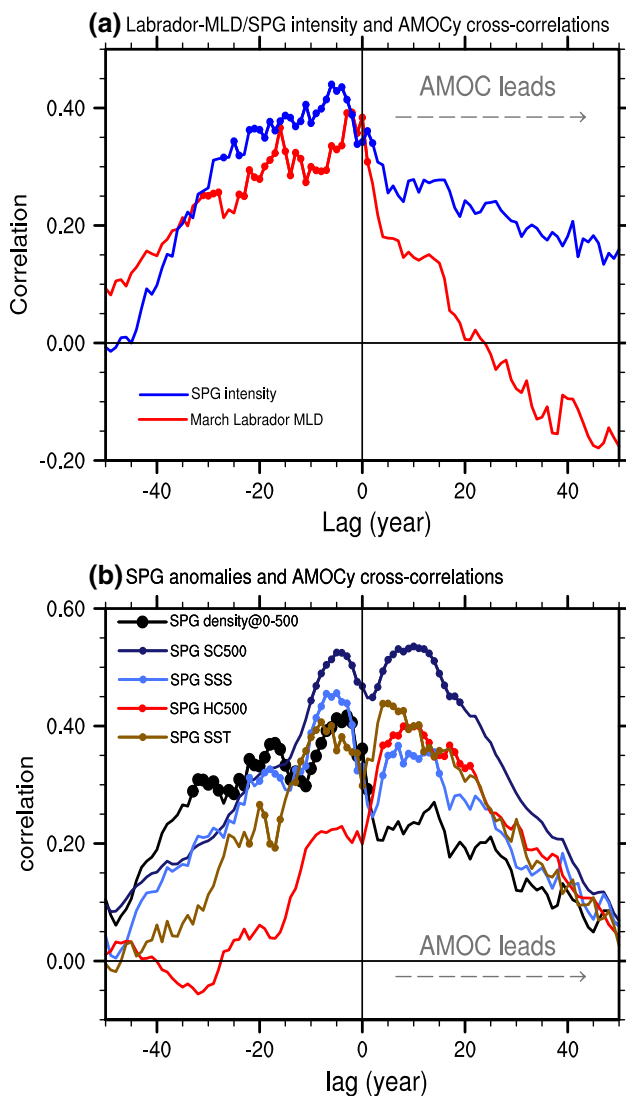


Fig. 8 **a** Lead-lag correlations between annual time series of SPG intensity/March mixed layer depth (MLD) over the Labrador Sea and AMOCy. Significance at the 95 % confidence level based on bootstrapping method is given by *plain dots*. Positive lags mean AMOC is leading. The SPG intensity index is based on the annual barotropic streamfunction averaged over the SPG region where climatological values are lower than -10 Sv. **b** Same but for SPG density averaged from 500 m to surface, SPG salt and heat content averaged from 500 m to surface, SSS and SST

except over the GIN Seas. Significance for the latter field is restricted to the Nordic Seas and south of 35°N from Lag -25 yr onwards (Fig. 6c–e) whereas the entire basin is almost covered by saltier water (Fig. 6h–j). Weaker signal in HC200 is associated with fluxes for both winter NAO+ and EAP+ that tends together to cool down the surface ocean along a broad 40°N – 60°N band (Fig. 7c, d). In addition, anomalous Ekman pumping associated with divergence of anomalous Ekman transport during EAP+ (Fig. 6a) tends to bring colder water from subsurface to the upper level ocean on the eastern side of the SPG. These

effects destructively interfere with the northward advection and invasion of warm water due to the acceleration of the SPG horizontal circulation (Fig. 8a) and the progressive increase of the AMOC. That said, their damping actions are not prominent enough to cancel out the overall warming due to the dynamical response of the ocean to winter NAO+ and EAP+ forcings. In addition, they cannot counteract the progressive densification due to the salinity perturbation and acceleration of the SPG via the internal S-feedback. This is consistent with studies dealing with periods of variability greater than a decade or so (e.g. Krahnemann et al. 2001). As a summary, Fig. 8b shows the respective contribution of heat and salt in the relationship between density in SPG and AMOC.

When NAO+ and EAP+ winter forcings stops around \sim Lag -20 yr, the entire North Atlantic Ocean from 35°N to the Arctic is saltier (Fig. 6d, j). Warming is very pronounced in the northward outer-rim of the SPG as well as in the GIN Seas except locally in the center where deep convection driven by salinity anomalies mixes colder water from depth (Fig. 6e, d). Warming is also present along the NAC in response to the spin up of the STG that transports heat anomalies from the tropics on its western side. On its eastern side, anomalous heat is found to propagate southwestward back to the tropics due to enhanced STG recirculation, from the African coast to the Caribbean as suggested by Fig. 3 (Lags -25 to -15 yrs). Accordingly, anomalous positive SST anomalies tend to spread out to the south with time while the northern basin continues warming. We now concentrate in the following section on the puzzling sign shifts of the NAO around -10 years while AMOC is still rising and of the winter EAP over the $(-5/+5)$ -yr window. Focus will be also laid on the summer EAP+ mode that is present prior to AMOC maximum.

6 Full development of the AMV and AMOC decline

In addition to the contribution of the recirculation branch of the STG in response to winter-induced adjustment as above-discussed, summer EAP+, which has been present since \sim Lag -30 (Fig. 5d), tends through surface fluxes (similar to their winter counterpart in Fig. 7d but divided by a factor of 10 at midlatitude and 2 along 30°N , not shown) to further warm the ocean in the subtropics from 20° to 35°N . This leads to the southwestward extension of positive SST anomalies. Note that EAP+ summer fluxes continue damping locally the warm heat anomalies generated by winter-induced ocean circulation changes around 50°N while they still act as a positive feedback for GIN. Although the amplitudes of the atmospheric forcings are much weaker in summertime, altered fluxes may have significant impacts at the near-surface ocean because of the

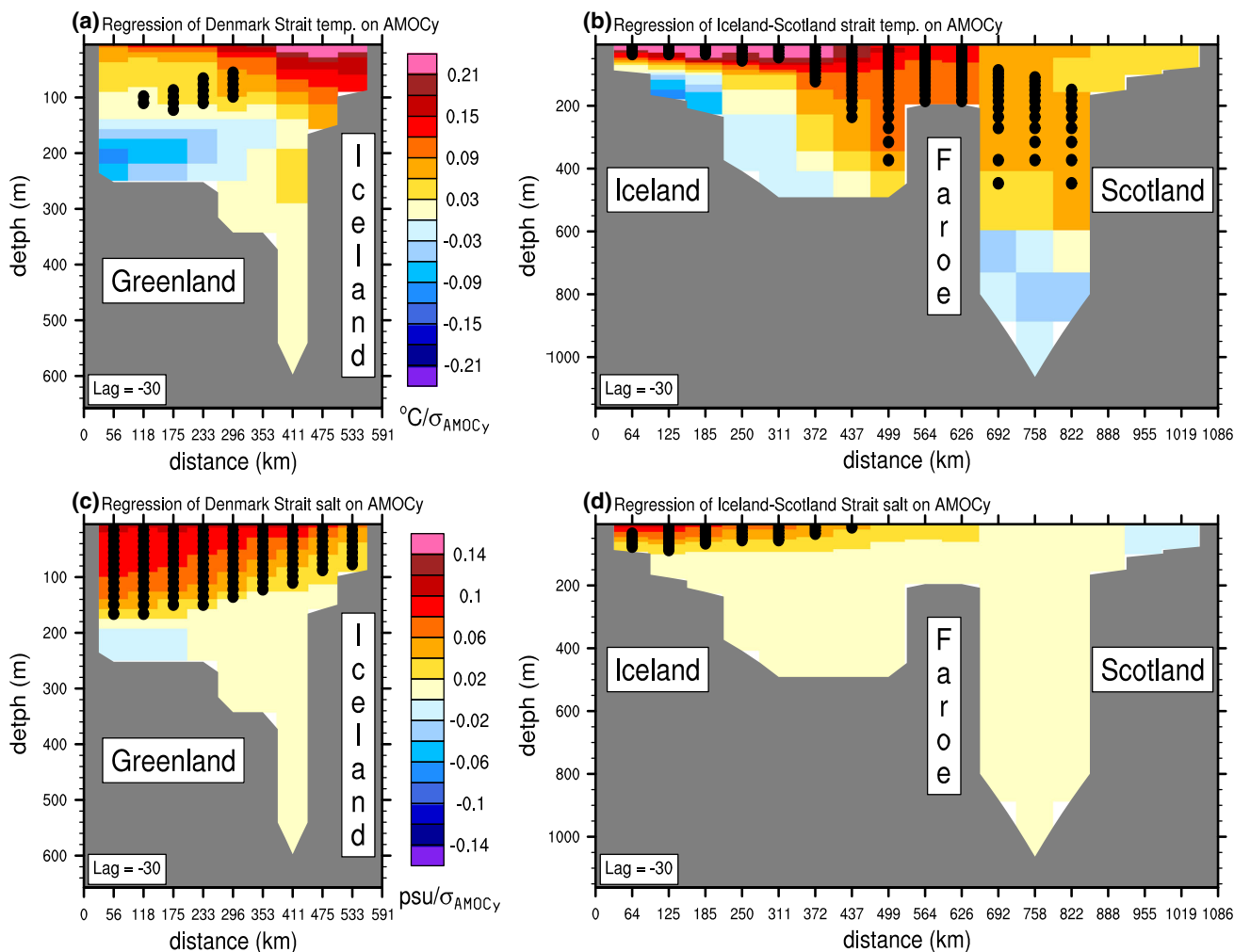


Fig. 9 Cross-sections of 5-yr running mean regressed temperature (upper panels, **a**, **b**) and salinity (lower panels, **c**, **d**) on 5-yr running mean AMOCy at Lag -30 yr for transects given in Fig. 1f and

corresponding to the Denmark Strait (left) and Iceland-Scotland Strait (right), respectively. Significance at the 95 % confidence level based on bootstrapping method is given by plain dots

seasonal very-shallow mixed layer depth, while wind forcing plays a minor role on the ocean dynamics for that season (e.g. Barrier et al. 2013).

The emergence for NAO- over the (-15/-3)-yr temporal window for both summer and winter seasons, albeit weakly significant (Fig. 5c), is concomitant with changes in the position/strength of the Atlantic Inter Tropical Convergence Zone (ITCZ). In agreement with several studies (e.g. Menary et al. 2012), enhanced AMOC in CNRM-CM5 and associated warmer surface imprints at large scale through the AMV build-up, is linked to increased summertime precipitation along a broad latitudinal band around 12°N leading to enhanced African monsoon while drought conditions prevails southward, especially in the northern portion of South America (Fig. 12a). The ITCZ shift starts about -15 yr before an AMOC maximum and persists up to ~Lag

+25 yr (not shown). Changes in the model Atlantic ITCZ is accompanying by the alteration of the summer global Hadley cell circulation that is clearly reinforced (especially its rising branch, in agreement with Fontaine et al. 1999; Zhang and Delworth 2005) and expands northward (Fig. 12b). We find that the NAO- anomalous pattern is more pronounced aloft than at the surface. Figure 12c displays the anomalous Z500* regressed pattern upon AMOCy index at Lag -10 yr (star standing for the departure from the zonal average of the geopotential height at 500 hPa) that is spatially correlated at -0.9 to the Z500* anomalous pattern which corresponds to the upper-level atmospheric signature of the summer NAO+. Z500* is preferred here to raw Z500 because the latter is polluted by the local expansion of the atmosphere due to the large-scale warming over the entire Atlantic, similarly to DelSole et al. (2011).

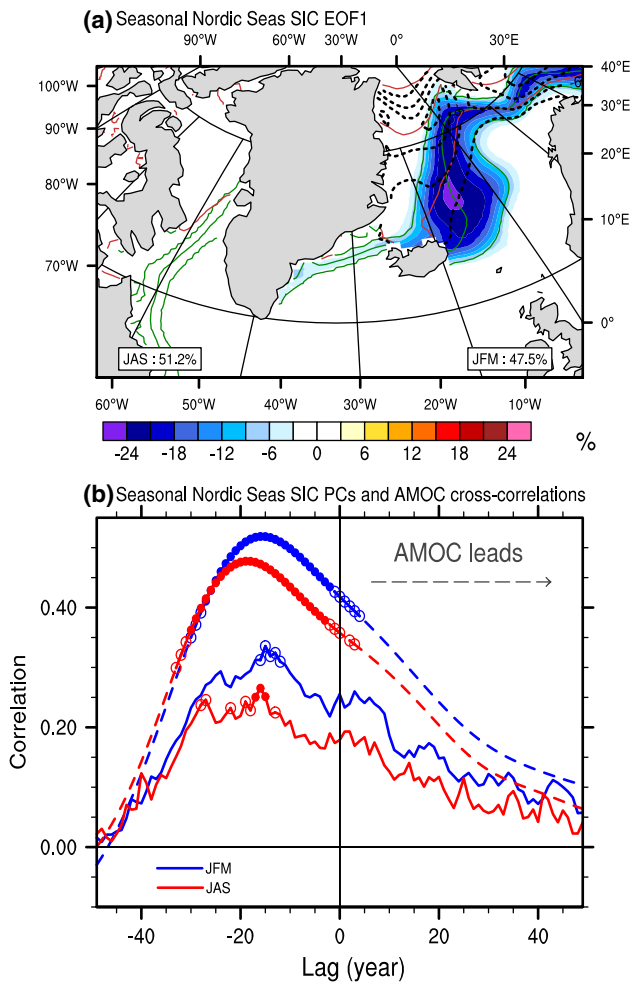


Fig. 10 **a** Leading EOF map of late winter (January–March, shading) and late summer (July–September, contour) sea-ice concentration (SIC). Percentages of explained variance are given in the lower corners. Climatological sea-ice cover is superimposed in green (winter) and brown (summer) (contour at 10, 50 and 90 % levels) **b** Lead-lag cross-correlations between seasonal raw/low pass filtered PCs and AMOCy/AMOC_PC (solid/dashed) indices. Significance at the 95 % (90 %) confidence level based on bootstrapping method is given by plain dots (circles). Positive lags mean AMOC is leading

Summertime NAO— is interpreted as the extratropical atmospheric response to changes of the ITCZ and not as a forcing for AMOC rise despite the fact that significant lagged correlations between NAO and AMOCy occur prior an AMOC maximum (Fig. 5b). From Lag -15 yr onwards (Fig. 3), the subtropical northern Atlantic basin is warm enough to trigger a tropical atmospheric response leading to changes at midlatitudes through teleconnections following for instance Okumura and Xie (2001) or Cassou et al. (2004b). Figure 13 lends further support for this hypothesis. An ITCZ index is built by averaging the model JJAS anomalous precipitation over a narrow latitudinal band (8°N–18°N) covering the mean position of the Atlantic ITCZ from the Caribbean to the Sahel. JJAS

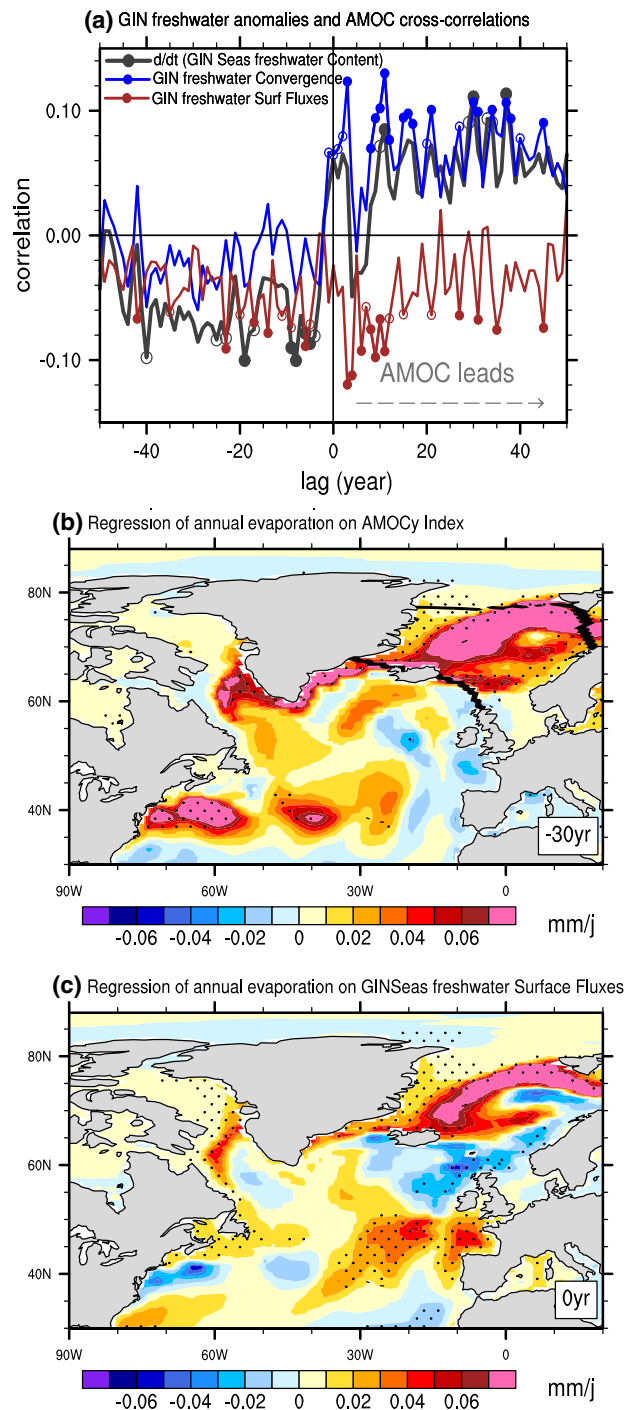


Fig. 11 **a** Lead-Lag correlation between AMOCy and the derivative of the GIN Seas total freshwater content (black), the surface total water flux (brown) and the oceanic freshwater convergence (blue). The GIN Seas domain used for the salinity budget is shown on **b**, its borders follow the PAGO transects. Significance at 95 % (90 %) confidence level based on bootstrapping method is given by plain dots (circles). Positive lags mean AMOC is leading. **b** Regression of the 5-yr running mean annual evaporation field on the 5-yr running averaged AMOCy index for Lag -30 yr. **c** In phase regression of the 5-yr running mean annual evaporation field on the 5-yr running averaged GIN Seas freshwater surface fluxes index. Stippling on **b** and **c** stands for significance based on bootstrapping at the 95 % confidence level

surface temperatures regressed upon this index (Fig. 13a) that is largely dominated by interannual to decadal variability, show warming in the northern subtropical Atlantic basin as part of a broad midlatitude horseshow pattern. Such as structure strongly resembles the one obtained from observations (e.g. Cassou et al. 2004b, their Fig. 2) and has been interpreted from sensitivity model experiments to be the surface ocean imprint of atmospheric forcing in response to ITCZ change. Regressed Z500* upon the ITCZ index projects very well onto the NAO pattern (spatial correlation equal to -0.7 with NAO+, Fig. 13b) but also onto the EAP one, to a lower extent (correlation equal to $+0.5$, not shown).

To even further lend some credibility to the diagnostic analyses presented so far, and to test the robustness of the interpretation that summertime NAO–/EAP+ excitation prior an AMOC maximum is indeed a response to slowly developing AMV and not a real forcing for AMOC rise, results from additional atmospheric GCM simulations are provided in Fig. 14. We use two sensitivity model experiments performed within the DYNAMITE project where ARPEGE is forced by the SST anomalies corresponding either to WARM or COLD phases of the observed AMV, (1951–1960) versus (1961–1990) mean conditions respectively. ARPEGE is integrated for 80 years for each experiments and the difference WARM–COLD is analyzed in the following. It would have been ideal to use here the CNRM-CM5 model AMV pattern to force ARPEGE instead of the observed one but both are strongly reminiscent (compare Fig. 14a, b) and we believe that the interpretations from DYNAMITE to understand the CNRM-CM5 processes are still valuable. The only concern stands for high latitudes because prescribed sea-ice anomalies in DYNAMITE reflect the observed trends that are mostly explained by anthropogenic forcing and are not consistent warm (1951–1960) decades characterized by greater ice than (1961–1990) ones, Fig. 14b) with the model AMV/ice relationship (Figs. 10, 14a). The reader is invited to refer to Hodson et al. (2011) where the experimental protocol and the main results are described in details.

In summer, the DYNAMITE SLP response to AMV is characterized by a basin-wide negative SLP anomaly with maximum loading located south of Iceland (Fig. 14c); the pattern projects very well on EAP+. To go beyond the simple evaluation of mean changes, we perform an EOF decomposition of the NAE SLP anomalies calculated from WARM and COLD concatenated experiments. Monthly anomalies for December–March months taken separately are preferred instead of DJFM seasonal means to increase the sample size (4 months \times 80 years \times 2 experiments) so that one can correctly draw the probability density functions (PDF) of the principal components for the two

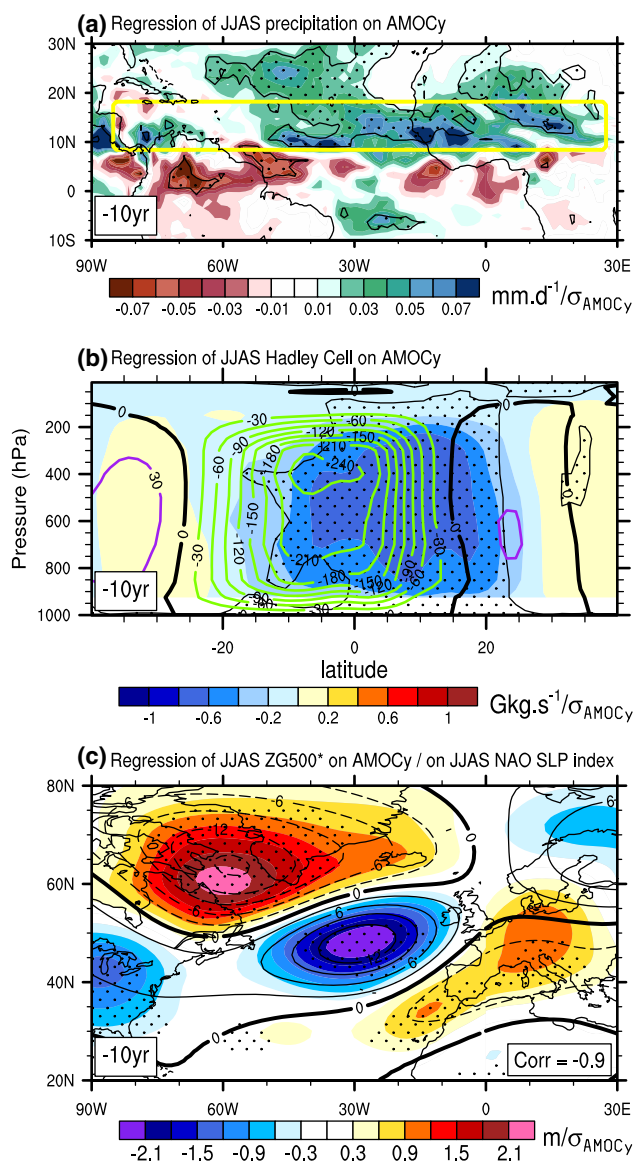


Fig. 12 Regression on 5-yr running averaged AMOCy at Lag -10 yr for summer (JJAS) 5-yr running mean precipitation (a), atmospheric meridional streamfunction (b) and eddy geopotential height at 500 hPa (c). Units are $\text{mm}\cdot\text{day}^{-1}$, $\text{Gkg}\cdot\text{s}^{-1}$, and meter per standard deviation of 5-yr running averaged AMOCy, respectively. Stippling stands for significance based on bootstrapping at the 95 % confidence level. Mean summer atmospheric meridional streamfunction (contour interval is $30 \text{ Gkg}\cdot\text{s}^{-1}$) is superimposed in b. The regression of JJAS Z500* on JJAS NAO estimated from EOF (Fig. 5a) is superimposed in c, contour interval is 3 m per standard deviation of PC. The spatial correlation between the two Z500* patterns is given in the lower right corner. Yellow box in a materializes the domain for averages of the precipitation ITCZ index

experiments. Shift in the PDF towards positive values is clear for the WARM experiments with respect to the COLD one for summer EAP (Fig. 14g); this is indicative for more excitation of summer EAP+ in response to positive AMV. These findings confirm that the statistical correlations found in Fig. 5d for EAP at negative lags must

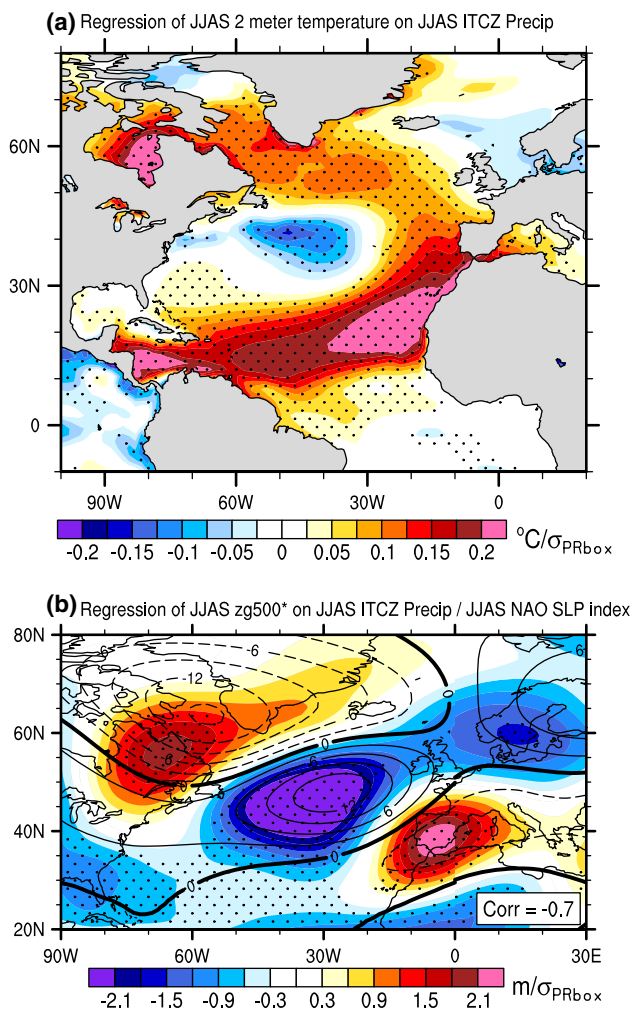


Fig. 13 Regression of JJAS 2-meter temperature (a) and eddy geopotential height at 500 hPa (b) on JJAS precipitation ITCZ index. Stippling stands for significance based on bootstrapping at the 95 % confidence level. The regression of JJAS Z500* on JJAS NAO estimated from EOF (Fig. 5a) is superimposed in b, contour interval is 3 m per standard deviation of PC. The spatial correlation between the two Z500* patterns is given in the *lower tight corner*

be interpreted as the local atmospheric response to the ongoing warming of the North Atlantic basin, and not as a direct forcing for AMOC. The EAP response to the ocean is consistent with theoretical works (e.g. Kushnir et al. 2002), model studies (e.g. Msadek and Frankignoul 2010), and observation (Sutton and Dong 2012). No significant change is found for the summer NAO in DYNAMITE (Fig. 14g). In winter, mean changes in DYNAMITE are reminiscent of a Rossby wave originating from the Caribbean basin and extending northeastward (Fig. 14d). For EAP, the PDF is shifted towards negative values suggestive for greater excitation of EAP– during warm AMV with respect to cold AMV (Fig. 14h). This again confirms that the sign shift for winter EAP in Fig. 5d at Lag (–5,+10)-yr must be treated as the atmospheric response to warm AMV.

Similarly to summertime, the NAO is not altered in winter (Fig. 14f). We believe that the mismatched AMV/ice forcing imposed in ARPEGE in DYNAMITE could alter the model local response by counteracting the emergence of higher geopotential height at polar latitudes in link to both summertime and wintertime NAO– when AMV is positive (Hodson et al. 2011, their Fig. 7). Cassou et al. (2004a, their Figs 5 and 8) lend some credit to this hypothesis because the ARPEGE model does favor NAO– regimes when the North Atlantic, and especially the tropical band, is warmer in agreement with other models when sea-ice is not changed (e.g. Sutton et al. 2001).

NAO– and EAP– have a positive feedback on AMV through surface heat fluxes (Fig. 7b, d), especially on SPG, and contribute to its full maturity, but they act simultaneously as a negative feedback on the AMOC strength because (1) induced SST warming of the SPG more and more counteracts the above-detailed driving influence of anomalous salinity and tends to inhibit any further intensification of deep convection. Figure 8a shows indeed that maximum correlation between SPG intensity/Labrador mix layer depth and AMOC is found around –5 yr before declining. Figure 8b reveals also that the SST warming of the SPG starts getting significant exactly when the NAO sign shift occurs around Lag –15/–10 yr while correlation values of the averaged temperature over the upper 500-m ocean (HC500) are still weak (Fig. 8b), (2) the GIN Seas route is stopped because of direct Ekman response to EAP– and because of local barotropic response of the GIN gyre to NAO–, both leading to a reduction of heat inflow through ISR (not shown), and finally because of reversed sign surface fluxes that now tend to cool down the surface ocean over this seas (Fig. 7b). Accordingly, ice reduction, even if AMOC is still rising, declines from Lag –15 yr onwards (Fig. 10b) and associated above-detailed positive salinity anomalies exported through Denmark Strait by EGC towards the Labrador Sea stops. (3) the direct ocean dynamical response to NAO– and EAP– wind anomalies leading to a southward retreat and slackening of the ocean circulation along the inter-gyre that tends to diminish the AMOC circulation (Fig. 7a, c). Downwelling occurring in SPG due to EAP– windstress curl anomalies is hypothesized to explain the warming of HC500 after the AMOC maximum over the (+3/+15)-yr window (Fig. 8b) in addition to the direct enhanced northward heat transport due to AMOC itself. The latter are responsible for a decrease in SPG density while salinity is still anomalous high. Note that in addition of (2), advection of fresher water from the Arctic basin through Fram Straits also appears from Lag –10 yr and starts eroding the excess of salt in GIN as diagnosed from a salinity budget (Fig. 11a). The emergence of fresher water is due to melting of Arctic sea ice as a whole (correlation between low-pass filtered

Fig. 14 Regression of the annual SST (*shading*) and JAS sea-ice concentration (SIC, *contour*) upon the AMV index of PiCTL (a). Contour interval for sea-ice is 2 % per standard deviation of AMV, *green* and *blue* for positive and negative values respectively. Annual SST and SIC pattern differences between the WARM and COLD ARPEGE forced experiments (b). WARM–COLD SLP difference for summer (c) and winter season (d). Contour interval is 0.2 hPa. Probability density functions for normalized NAO indices e, f for summer (e) and winter seasons (f) for WARM (*red*) and COLD (*blue*) experiments taken separately. g, h Same but for EAP

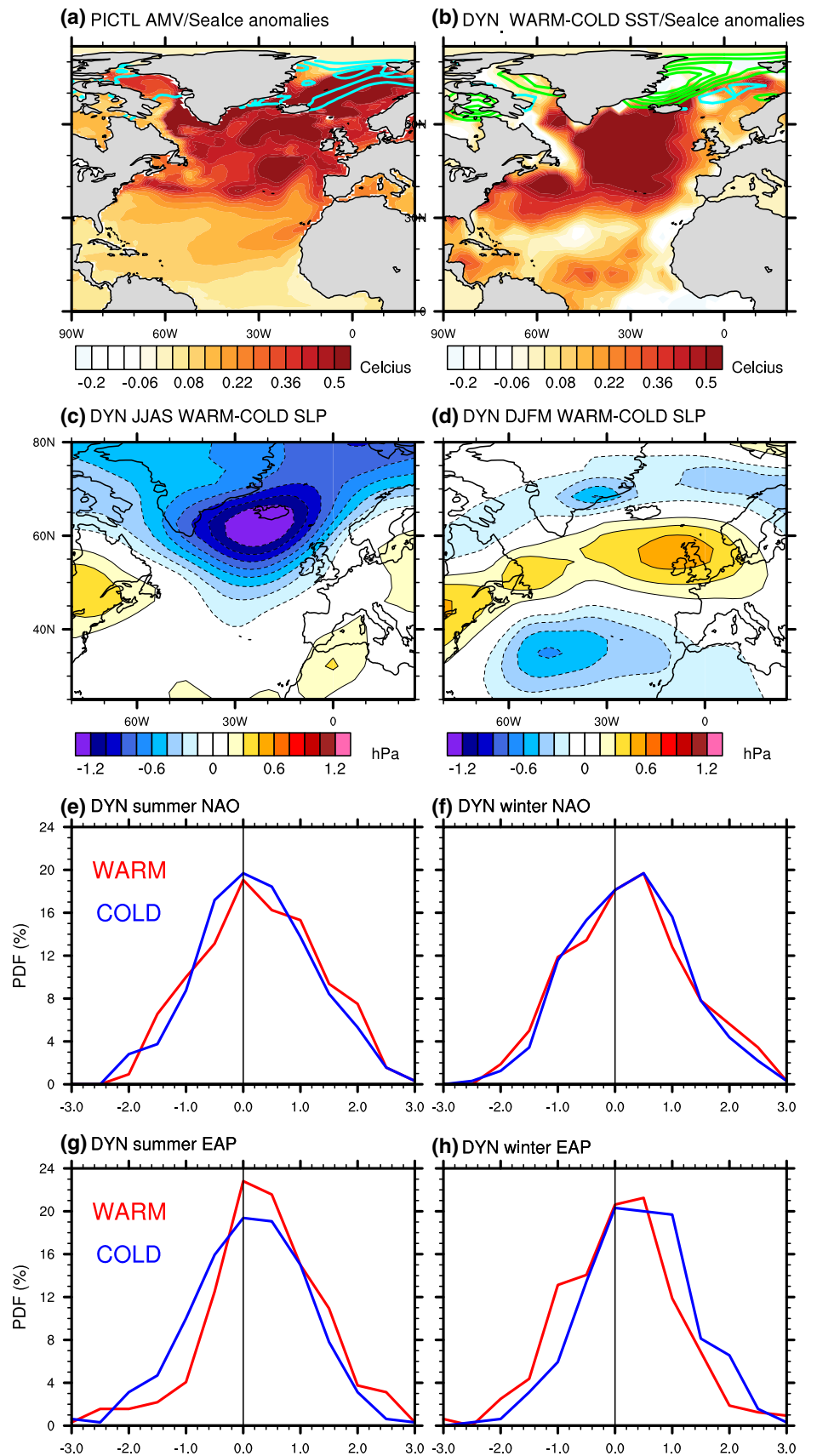
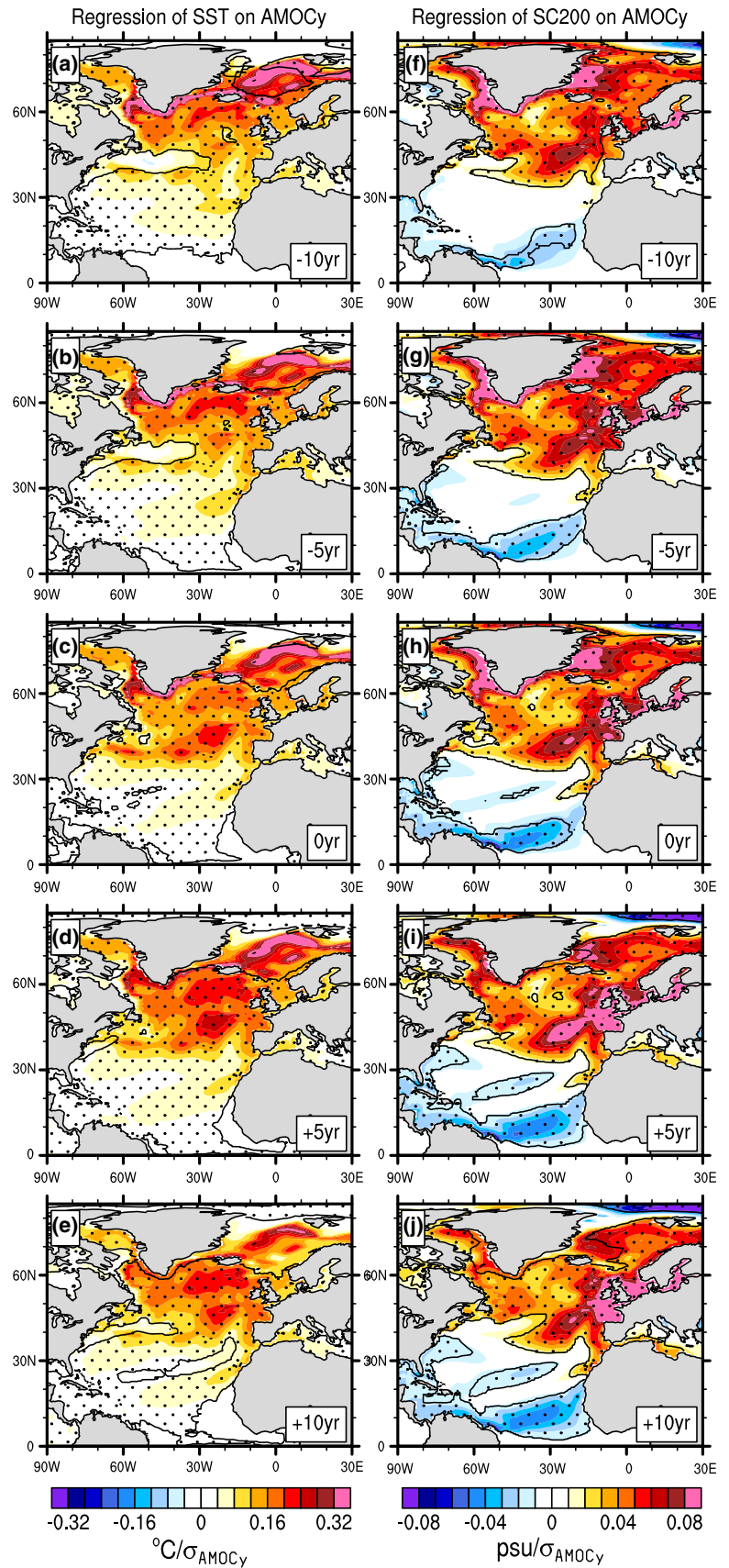


Fig. 15 Same as Fig. 6 but for SST (left panels) and salt content (right panels)



Arctic sea-ice volume and AMOC_PC equal to 0.65) in link to warmer atmospheric conditions at polar latitudes when AMV is positive. These negative salt anomalies further contribute to the damping of AMOC episodes.

This sequence of events can be tracked in Fig. 15. While SST in SPG keeps warming (Fig. 15a–e), significance is lost from Lag -10 yr onwards in the GIN Seas despite strong residual positive anomalies and this loss gradually propagates along the EGC. SC200 anomalies in GIN Seas behave similarly and progressively diminish (Figs. 11a, 15f–j); from Lag $+5$ yr onwards, fresher water tends to recirculate along the local GIN Seas gyre from its southwestern side (loss of significance north of Iceland) while strong negative anomalies appear in the northernmost region. Note that at Lag 0 (Fig. 15c, h), the damping mechanisms at work are appearing to be on hold because of the imprint of the fast response of the ocean to atmospheric forcing (Msadek and Frankignoul 2009) that pollutes the multidecadal processes documented in this paper.

In addition to NAO–/EAP– and the export of negative salinity anomalies from the deep Arctic, the emergence of fresher water in the northern tropical Atlantic and its progressive northward advection by the mean western boundary circulation also acts as negative feedback for AMOC. SC200 anomalies appear from \sim Lag -10 yr along the 10°N – 20°N latitudinal band (Fig. 15f) and are associated with increased freshwater flux due to stronger ITCZ and with reduced evaporation due to concurrent slackened trade winds. We verified that subsurface and surface salinity anomalies are homogeneous over the vertical levels used for SC200 computation while subsurface and surface temperature anomalies are strongly anti-correlated due to thermocline slope anomalies, in agreement with Zhang (2007). Advection along the mean barotropic circulation (Fig. 1d) can be easily followed in Fig. 15g, h where the entire Caribbean basin is slowly invaded by fresh water anomalies whose amplitude gets significant with lags, before being exported northward by the NAC (Fig. 15i, j) leading to a progressive erosion of the saline anomalies standing there. This mechanism has been demonstrated in other GCMs as presented for instance in Vellinga and Wu (2004), Menary et al. (2012) or from sensitivity experiments where artificial freshening of the tropical Atlantic basin is imposed (Mignot and Frankignoul 2010). Concurrently, acceleration of mean western boundary circulation in the northern tropical basin occurs as a response to an AMOC event (not shown), and amplifies the negative feedback associated with the emergence of the subtropical freshwater anomalies. Note though that compared to Vellinga and Wu (2004), the fresher water advected from the tropics are not strong enough in CNRM-CM5 to invert the SPG salinity anomalies and trigger an oscillation.

7 Summary and discussion

The spatio-temporal characteristics of the AMV and associated physical processes have been investigated in a 1,000-yr control simulation of CNRM-CM5. Low-frequency fluctuations of the AMOC are shown to be the main precursor for AMV events in the model. Maximum loading is found at multidecadal-to-centennial timescale accounting for about 40 % of the total North Atlantic yearly-averaged SST variability. We suggest that AMOC events and subsequent AMV are mostly driven by the low-frequency portion of the white spectrum of the wintertime NAE atmospheric modes of variability. This interpretation for multidecadal AMV is consistent with other studies (e.g. Delworth and Greatbatch 2000; Dong and Sutton 2005) despite the fact that the precise timescales of the ocean–atmosphere relationship and the precise AMV properties differ among the papers; such discrepancies might be explained by the own characteristics of the models (resolution, oceanic convection scheme, spatio-temporal properties of the atmospheric internal modes of extratropical variability, tropical–extratropical teleconnection etc.). The full life cycle of AMOC/AMV events in CNRM-CM5 relies on a complex combination of NAO and EAP influences that must be considered from a seasonal perspective; the ocean is responsible for setting the timescale.

Through a diagnostic approach, we find, as summarized in Fig. 16, that an AMOC maximum leading to a warm phase of the AMV, is preceded by:

1. Positive wintertime NAO and EAP whose wind-stress anomalies lead to (1) an acceleration of the gyre circulations (especially the SPG) and of the NAC. The latter increases the northward transport of warm and saline waters from the eastern side of the SPG (hereafter the southern route) into the region of active deep convection that is progressively reinforced. (2) additional inflow of warm waters into the GIN Seas through ISR that inhibits sea-ice formation there in both winter and summer seasons in combination to direct surface fluxes from NAO+ and EAP+. Enhanced evaporation associated with ice-free zones is the dominant term of the altered surface freshwater budget leading to positive salinity anomalies that are advected along the EGC towards the Labrador Sea (hereafter the northern route). The combined effect of the southern (1) and northern (2) routes efficiently contributes to the progressive densification through salinization and acceleration of the SPG following the so-called internal salinity feedback, leading *in fine* to AMOC rise. Wintertime NAO and EAP stimulation is active over the 40-to-25 yr temporal window prior to an AMOC maximum. Based on sensitivity experiments

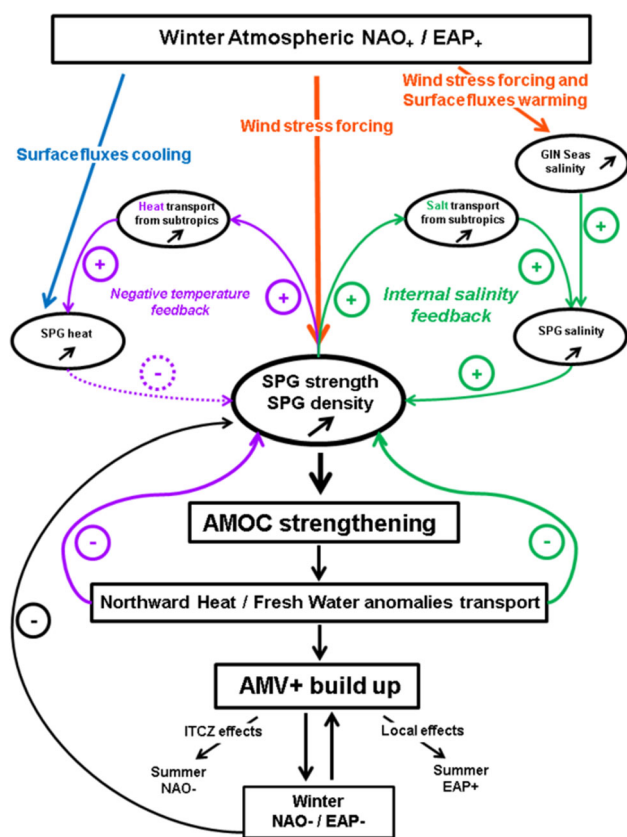


Fig. 16 Schematic diagram for a typical AMOC/AMV positive event

using the same ocean component as in CNRM-CM5 but in a forced-mode, Barrier et al. (2013) suggests that the dynamical ocean response to NAO and EAP is mostly controlled by the action of the wind and secondarily by the surface fluxes. In fact, the latter in CNRM-CM5 tend to damp the heat excess advected into the SPG from the southern route so that the salinity factor controls most of circulation changes in the model midlatitude Atlantic Ocean. However, altered fluxes by EAP tend to warm up the subtropical basin and reinforce the positive SST anomalies produced by the recirculation of warmer water from the eastern side of the basin along the enhanced STG.

2. Positive summertime EAP for lags spanned from -30 to $+10$ years. Summer EAP+ is shown from additional AGCM experiments to be a response of the atmosphere to local warmer large-scale conditions of the mid- and high-latitude Atlantic basin in agreement with theory (Kushnir et al. 2002) and literature (e.g. Msadek and Frankignoul 2009; Hodson et al. 2011). This weak coupling contributes to further warm the GIN Seas and the subtropical basin through surface heat fluxes. The wind driving action of the ocean dynamics is minor in summertime.

3. Preferred negative summertime and wintertime NAO for lags greater than -15 years, albeit with weak statistical significance. NAO- is interpreted as the atmospheric response to warmer tropical North Atlantic basin through teleconnection in link to the intensification of the ITCZ. NAO- acts as a positive feedback for the full development of the AMV through surface heat fluxes but at the same time prepares its termination through negative retroaction on AMOC. The ocean dynamical response to wintertime NAO- leads to a slackening of the AMOC. Strong surface warming of the SPG during NAO-, because of local reduced turbulent fluxes, tends to inhibit ocean deep convection and eventually counteracts the established salinity effect of opposite sign. In addition, cooling in the GIN Seas through the enhanced advection of colder air from the Arctic during NAO- tends to reform sea-ice and cuts the northern route.
4. Excitation of winter EAP- at the peak of AMOC/AMV. The oceanic response leads to enhance heat invasion (Ekman pumping) and surface warming in the SPG leading to a decrease of density.

All together, the combined effect of NAO and EAP, their seasonal particularities and their intertwined forcing/forced role upon/by the ocean are responsible in CNRM-CM5 for an irregular and damped mode of variability of AMOC/AMV that takes about 35–40 years to build up and about 15–20 years to dissipate. In addition to the direct NAO-/EAP- action, the termination of AMOC/AMV events is also induced by the advection of anomalous fresh water from the subtropical North Atlantic basin along the mean western boundary ocean circulation as found in many models (e.g. Jackson and Vellinga 2013), and also from the Arctic due to considerable ice volume loss associated with overall atmospheric warmer conditions when AMOC is enhanced.

It is extremely complex from the sole PiCTL experiment to evaluate the respective weight of all the processes and feedbacks documented here. Using OGCM (Barrier et al. 2013) and AGCM (Hodson et al. 2011) sensitivity experiments based on the same ocean and atmospheric components respectively, we have tried to list and deconvolute at best the different actors without firmly conclude if they are all strictly necessary to sustain the AMOC fluctuations. Predictability experiments have been conducted as well. Two specific dates corresponding to strong and weak AMOC extremes, year 141 and year 303 in PiCTL respectively (Fig. 4), have been selected and ensemble simulations have been carried out to evaluate the predictability level and associated mechanisms. Processes reported in this paper leading to AMOC decline are confirmed in these experiments especially the role of the advection of

salinity from the tropics as well as the GIN Seas influences. Weak coupling with wintertime NAO–/EAP– leading to a slackening of the AMOC is also found in the predictability experiments in line with Gastineau and Frankignoul (2012). The role of the model biases in determining the chain of events presented in the paper is a legitimate question at that point. We think that the biases in the ocean dynamics can affect the temporal characteristics of the AMOC but not the overall behavior of the model variability. The AMV pattern in CNRM-CM5 bears some resemblance with the observed one and its association with summertime EAP and both seasons NAO– combined to changes in the ITCZ appears to be fairly realistic (Sutton and Dong 2012, their Fig. 4 for summer).

The present paper documents AMV/AMOC physical processes mostly from a linear approach (lead-lag regressions etc.). Additional analyses, beyond the scope of this paper, seem to suggest though that asymmetries with respect to the phase of the AMV might be considered for some specific aspects. The stationarity of the ocean–atmosphere relationship should be also tackled since diagnostics are presented here over the full 1,000-yr period of PiCTL. We showed that the GIN Seas plays an active role on average but the weight of the latter depends on its preconditioning and especially on its level of sea-ice cover in link to global Arctic low-frequency climate fluctuation. Part of it is related to IPV whose connections with AMV is clearly non-stationary (not shown) as assessed when the 1,000-yr run is chunked into 100-yr period to match the observational record length. The present paper appears to be essential though to better understand the model performance when used in decadal forecast mode and in particular to document the physical mechanisms at the origin of the high predictability level of CNRM-CM5 in the Atlantic as shown in the Bellucci et al. (2014) intercomparison paper.

Acknowledgments The authors are very grateful to Julie Dehayes for having computing ocean transects used in our study and Elodie Fernandez for her help in handling model outputs. We thank Laurent Terray for stimulating discussion and Juliette Mignot, Hervé Douville and Laurent Dubus for their suggestions. Thanks to the two anonymous reviewers whose comments clearly helped improving the manuscript. The figures were produced with the NCAR Command Language (NCL) Software (doi:10.5065/D6WD3XH5NCL). This work was supported by Cerfacs, CNRS, EDF and GICC (Gestion des Impacts du Changement Climatique) via the EPIDOM project under contract 10-MCGOT-GICC-7-CVS-131.

References

- Bellucci A et al (2014) An assessment of a multi-model ensemble of decadal climate predictions. *Clim Dyn*. doi:10.1007/s00382-014-2164-y
- Danabasoglu G et al (2014) North Atlantic simulations in coordinated Ocean-ice reference experiments phase II (CORE-II). Part I: mean states. *Ocean Model*. doi:10.1016/j.ocemod.2013.10.005
- Voltaire A et al (2013) The CNRM-CM5.1 global model: description and basic evaluation. *Clim Dyn*. doi:10.1007/s00382-011-1259-y
- Zhang R et al (2013) Have aerosols caused the observed Atlantic multidecadal variability? *J Atmos Sci*. doi:10.1175/JAS-D-12-0331.1
- Antonov JJ, Locarnini RA, Boyer TP, Mishonov AV, Garcia HE (2006) World Ocean Atlas 2005, vol 2: salinity. In Levitus S (ed) NOAA Atlas NESDIS 62, US Government Printing Office, Washington, DC
- Barnston AG, Livezey RE (1987) Classification, seasonality and persistence of low-frequency atmospheric circulation patterns. *Mon Wea Rev* 115:1083–1126
- Barrier N, Cassou C, Treguier AM, Deshayes (2013) Response of North-Atlantic Ocean circulation to atmospheric weather regimes. *J Phys Ocean*. doi:10.1175/JPO-D-12-0217.1
- Bentsen M, Drange H, Furevik T, Zhou T (2004) Simulated variability of the Atlantic meridional overturning circulation. *Clim Dyn* 22:701–720
- Biastoch A, Böning CW, Getzlaff J, Molines JM, Madec G (2008) Causes of interannual-decadal variability in the meridional overturning circulation of the midlatitude North Atlantic Ocean. *J Clim* 21:6599–6615
- Booth BBB, Dunstone NJ, Halloran PR, Andrews T, Bellouin N (2012) Aerosols implicated as a prime driver of twentieth-century North Atlantic climate variability. *Nature* 484:228–232
- Born A, Mignot J (2012) Dynamics of decadal variability in the Atlantic subpolar gyre: a stochastically forced oscillator. *Clim Dyn*. doi:10.1007/s00382-011-1180-4
- Brambilla E, Talley LD (2008) Subpolar mode water in the northeastern Atlantic: 1. Averaged properties and mean circulation. *J Geophys Res* 113:C04025. doi:10.1029/2006JC004062
- Cassou C, Terray L, Hurrell JW, Deser C (2004a) North Atlantic winter climate regimes: spatial asymmetry, stationarity with time and oceanic forcing. *J Clim* 17:1055–1068
- Cassou C, Deser C, Terray L, Hurrell JW, Drévillon M (2004b) Summer sea surface temperature conditions in the north atlantic and their impact upon the atmospheric circulation in early winter. *J Clim* 17:3349–3363
- Chang CY, Chiang JCH, Wehner MF, Friedman AR, Ruedy R (2011) Sulfate aerosol control of tropical Atlantic climate over the twentieth century. *J Clim* 24(10):2540–2555
- Chiang JCH, Cjng CY, Wehner MF (2013) Long-term behavior of the Atlantic Interhemispheric SST gradient in the CMIP5 historical simulations. *J Clim* 26:8628–8640
- Cunningham SA et al (2007) Temporal variability of the Atlantic Meridional Overturning circulation at 26.5°N. *Science* 317:938–945
- Danabasoglu G (2008) On multi-decadal variability of the Atlantic meridional overturning circulation in the community climate system model version 3 (CCSM3). *J Clim* 21:5524–5544
- Davison AC, Hinkley DV (1997) Bootstrap methods and their application. Cambridge University Press, Cambridge
- de Boyer Montégut C, Madec G, Fischer AS, Lazar A, Iudicone D (2004) Mixed layer depth over the global ocean: an examination of profile data and a profile-based climatology. *J Geophys Res* 109:C12003. doi:10.1029/2004JC002378
- DelSole T, Tippett MK, Shukla J (2011) A significant component of unforced multidecadal variability in the recent acceleration of global warming. *J Clim* 24:909–926
- Delworth TL, Greatbatch RJ (2000) Multidecadal thermohaline circulation variability driven by atmospheric surface flux forcing. *J Clim* 13:1481–1495
- Delworth TL, Mann ME (2000) Observed and simulated multidecadal variability in the Northern Hemisphere. *Clim Dyn* 16:661–676
- Delworth TL, Manabe S, Stouffer R (1993) Interdecadal variations of the thermohaline circulation in a coupled ocean–atmosphere model. *J Clim* 6:1993–2011

- Déqué M, Dreveton C, Braun A, Cariolle D (1994) The ARPEGE-IFS atmosphere model: a contribution to the French community climate modelling. *Clim Dyn* 10:249–266
- Deser C, Knutti R, Solomon S, Phillips AS (2012) Communication of the role of natural variability in future North American climate. *Nat Clim Change* 2:775–779. doi:[10.1038/nclimate1562](https://doi.org/10.1038/nclimate1562)
- Deshayes J, Frankignoul C (2008) Simulated variability of the circulation in the North Atlantic from 1953 to 2003. *J Clim* 21:4919–4930
- Deshayes J, Curry R, Msadek M (2014) CMIP5 model inter-comparison of freshwater budget and circulation in the North Atlantic. *J Clim* 27:3298–3317
- Dong B, Sutton RT (2005) Mechanism of interdecadal thermohaline circulation variability in a coupled ocean–atmosphere GCM. *J Clim* 18:1117–1135
- Duchon C (1979) Lanczos filtering in one and two dimensions. *J Appl Meteorol* 1016–1022
- Eden C, Willebrand J (2001) Mechanism of interannual to decadal variability of the North Atlantic circulation. *J Clim* 14:2266–2280
- Enfield D, Mestas-Nunez A, Trimble P (2001) The Atlantic multidecadal oscillation and its relation to rainfall and river flows in the continental U.S. *Geophys Res Lett* 28:2077–2080
- Folland CK, Colman AW, Rowell DP, Davey MK (2001) Predictability of northeast Brazil rainfall and real-time forecast skill, 1987–98. *J Clim* 14:1937–1958
- Fontaine B, Janicot S, Roucou P (1999) Coupled ocean–atmosphere surface variability and its climate impacts in the tropical Atlantic region. *Clim Dyn* 15:451–473
- Ganachaud A, Wunsch C (2000) The oceanic meridional overturning circulation, mixing, bottom water formation, and heat transport. *Nature* 408:453–457
- Gastineau G, Frankignoul C (2012) Cold-season atmospheric response to the natural variability of the Atlantic meridional overturning circulation. *Clim Dyn* 39(1–2):37–57
- Goldenberg SB, Landsea CW, Mestas-Nuñez AM, Gray WM (2001) The recent increase in Atlantic hurricane activity: causes and implications. *Science* 293:474–479
- Graham JA, Stevens DP, Heywood KJ, Wang Z (2011) North Atlantic climate responses to perturbations in Arctic Intermediate Water. *Clim Dyn* 37:297–311
- Gray ST, Graumlich LJ, Betancourt JL, Pederson GT (2004) A tree-ring based reconstruction of the Atlantic Multidecadal Oscillation since 1567 A.D. *Geo Res Lett* 31:L12205. doi:[10.1029/2004GL019932](https://doi.org/10.1029/2004GL019932)
- Griffies SM, Tziperman E (1995) A linear thermohaline oscillator driven by stochastic atmospheric forcing. *J Clim* 8:2440–2453
- Griffies SM et al (2009) Coordinated ocean-ice experiments (COREs). *Ocean Mod* 26:1–46. doi:[10.1016/j.ocemod.2008.08.007](https://doi.org/10.1016/j.ocemod.2008.08.007)
- Guemas V, Salas-Melia D (2008) Simulation of the Atlantic Meridional Overturning circulation in an Atmosphere-Ocean global coupled model. Part I: a mechanism governing the variability of ocean convection in a preindustrial experiment. *Clim Dyn* 31:29–48. doi:[10.1007/s00382-007-0336-8](https://doi.org/10.1007/s00382-007-0336-8)
- Gupta AS, Muir LC, Brown JN, Phipps SJ, Durack PJ, Monselesan D, Wijffels SE (2012) Climate drift in the CMIP3 models. *J Clim* 25:4621–4640
- Hakkinen S, Rhines PB (2004) Decline of subpolar North Atlantic Circulation during the 1990s. *Science* 304:555
- Hakkinen S, Rhines PB, Worthen DL (2011) Atmospheric blocking and Atlantic Multidecadal Ocean variability. *Science* 3334:655–659
- Hawkins E, Sutton R (2007) Variability of the Atlantic thermohaline circulation described by three-dimensional empirical orthogonal functions. *Clim Dyn* 29:745–762
- Hawkins E, Sutton R (2012) Time of emergence of climate signals. *Geophys Res Lett*. doi:[10.1029/2011GL050087](https://doi.org/10.1029/2011GL050087)
- Hegerl G, Zwiers F, Braconnot P, Gillet N, Luo Y, Marengo Orsini J, Nicholls N, Penner J, Stott P (2007) Understanding and attributing climate change. In: Solomon S et al (eds) *Climate change 2007: the physical science basis*, Cambridge University Press, Cambridge, pp 663–745
- Hodson DLR, Sutton RT (2012) The impact of resolution on the adjustment and decadal variability of the Atlantic meridional overturning circulation in a coupled climate model. *Clim Dyn* 39:3057–3073. doi:[10.1007/s00382-012-1309-0](https://doi.org/10.1007/s00382-012-1309-0)
- Hodson DLR, Sutton RT, Cassou C, Keenlyside N, Okumura Y, Zhou T (2011) Climate impacts of recent multidecadal changes in Atlantic Ocean Sea surface temperature: a multimodel comparison. *Clim Dyn* 34(7–8):1041–1058. doi:[10.1007/s00382-009-0571-2](https://doi.org/10.1007/s00382-009-0571-2)
- Hurrell JW, Kushnir Y, Otterson G, Visbeck M (2003) An overview of the North Atlantic Oscillation. *The North Atlantic Oscillation: climate significance and environmental impact*. *Geophys Monogr* 134 (American Geophysical Union 1:35)
- Jackson L, Vellinga M (2013) Multidecadal to centennial variability of the AMOC: HadCM3 and a perturbed physics ensemble. *J Clim* 26:2390–2407
- Jungclauss J, Haak H, Latif M, Mikolajewicz U (2005) Arctic-North Atlantic interactions and multi-decadal variability of the meridional overturning circulation. *J Clim* 18:4013–4031
- Kerr RA (2000) A North Atlantic climate pacemaker for the centuries. *Science* 288:1984–1985
- Knight JR (2009) The Atlantic multidecadal oscillation inferred from the forced climate response in coupled general circulation models. *J Clim* 22:1610–1625. doi:[10.1175/2008JCLI2628.1](https://doi.org/10.1175/2008JCLI2628.1)
- Knight JR, Allan RJ, Folland CK, Vellinga M, Mann ME (2005) A signature of persistent natural thermohaline circulation cycles in observed climate. *Geophys Res Lett* 32:L20708. doi:[10.1029/2005GL024233](https://doi.org/10.1029/2005GL024233)
- Krahmann G, Visbeck M, Reverdin G (2001) Formation and propagation of temperature anomalies along the North Atlantic Current. *J Phys Oceanogr* 31:1287–1303
- Kushnir Y, Robinson WA, Bladé I, Hall NMJ, Peng S, Sutton R (2002) Atmospheric GCM Response to extratropical SST anomalies: synthesis and evaluation. *J Clim* 15:2233–2256
- Kwon YO, Frankignoul C (2012) Stochastically-driven multidecadal variability of the Atlantic meridional overturning circulation in CCSM3. *Clim Dyn* 38:859–876
- Levermann A, Born A (2007) Bistability of the Atlantic subpolar gyre in a coarse-resolution model. *Geophys Res Lett* 34:L24605
- Locarnini RA, Mishonov AV, Antonov JI, Boyer TP, Garcia HE (2006) *World Ocean Atlas 2005, vol 1: temperature*. In Levitus S (ed) *NOAA Atlas NESDIS 61*, U.S. Government Printing Office, Washington, DC
- Lucarini V, Ragone F (2011) Energetics of PCMDI/CMIP3 climate models: energy budget and meridional enthalpy transport. *Rev Geophys* 49:RG1001. doi:[10.1029/2009RG000323](https://doi.org/10.1029/2009RG000323)
- Madec G (2008) NEMO ocean engine. *Note du Pole de modélisation, Institut Pierre-Simon Laplace (IPSL), France, No 27* ISSN No 1288–1619
- Marini C, Frankignoul C, Mignot J (2011) Links between the southern annular mode and the Atlantic Meridional Overturning Circulation in a climate model. *J Clim* 24(3):624–640
- Marshall J, Johnson H, Goodman J (2001) A study of the interaction of the North Atlantic Oscillation with ocean circulation. *J Clim* 14:1399–1421
- McCabe G, Palecki M, Betancourt J (2004) Pacific and Atlantic Ocean influences on multi-decadal drought frequency in the United States. *Proc Natl Acad Sci* 101:4136–4141

- Medhaug I, Furevik T (2011) North Atlantic 20th century multidecadal variability in coupled climate models: sea surface temperature and ocean overturning circulation. *Ocean Sci* 7:389–404. doi:[10.5194/os-7-389-2011](https://doi.org/10.5194/os-7-389-2011)
- Medhaug I, Langehaug HR, Eldevik T, Furevik T (2011) Mechanisms for multidecadal variability in a simulated Atlantic Meridional Overturning Circulation. *Clim Dyn* 39:77–93. doi:[10.1007/s00382-011-1124-z](https://doi.org/10.1007/s00382-011-1124-z)
- Meehl G, Goddard L, Murphy J, Stouffer RJ, Boer G, Danabasoglu G, Dixon K, Giorgetta MA, Greene AM, Hawkins E, Hegerl G, Karoly D, Keenlyside N, Kimoto M, Kirtman B, Navarra A, Pulwarty R, Smith D, Stammer D, Stockdale T (2009) Decadal prediction can it be skilful? *Bull Am Meteorol Soc*. doi:[10.1175/2009BAMS2778.1](https://doi.org/10.1175/2009BAMS2778.1)
- Meehl GA, Arblaster JM, Fasullo J, Hu A, Trenberth KE (2011) Model-based 595 evidence of deep ocean heat uptake during surface temperature hiatus periods. *Nature Clim Change* 1:360–364. doi:[10.1038/NCLIMATE1229](https://doi.org/10.1038/NCLIMATE1229)
- Meinen CS, Baringer MO, Garcia RF (2010) Florida current transport variability: an analysis of annual and longer-period signals. *Deep Sea Res Part I Oceanogr Res Pap* 57(7):835–846
- Menary BMB, Park W, Lohmann K, Vellinga M, Palmer MD, Latif M, Junclaus JH (2012) A multimodel comparison of centennial Atlantic meridional overturning circulation variability. *Clim Dyn* 38:2377–2388. doi:[10.1007/s00382-011-1172-4](https://doi.org/10.1007/s00382-011-1172-4)
- Mignot J, Frankignoul C (2005) The variability of the Atlantic meridional overturning circulation, the North Atlantic Oscillation, and the El Niño–Southern Oscillation in the Bergen climate model. *J Clim* 18:2361–2375
- Mignot J, Frankignoul C (2010) Local and remote impacts of a tropical Atlantic salinity anomaly. *Clim Dyn* 35:1133–1147
- Mohino E, Janicot S, Bader J (2011) Sahel rainfall and decadal to multi-decadal sea surface temperature variability. *Clim Dyn*. doi:[10.1007/s00382-010-0867-2](https://doi.org/10.1007/s00382-010-0867-2)
- Msadek R, Frankignoul C (2009) Atlantic multidecadal oceanic variability and its influence on the atmosphere in a climate model. *Clim Dyn* 33:45–62. doi:[10.1007/s00382-008-0452-0](https://doi.org/10.1007/s00382-008-0452-0)
- Msadek R, Frankignoul C (2010) Mechanisms of the atmospheric response to North Atlantic multidecadal variability: a model study. *Clim Dyn*. doi:[10.1007/s00382-010-0958-0](https://doi.org/10.1007/s00382-010-0958-0)
- Nilsen JEØ, Gao Y, Drange H, Furevik T, Bentsen M (2003) Simulated North Atlantic–Nordic Seas water mass exchanges in an isopycnic coordinate OGCM. *Geophys Res Lett* 30(10):1536. doi:[10.1029/2002GL016597](https://doi.org/10.1029/2002GL016597)
- Noilhan J, Planton S (1989) A simple parameterization of land surface processes for meteorological models. *Mon Wea Rev* 117:536–549
- Oki T, Sud YC (1998) Design of total runoff integrating pathways (TRIP). A global river channel network. *Earth Interact* 2:1–36
- Okumura Y, Xie SP (2001) Tropical Atlantic air–sea interaction and its influence on the NAO. *Geophys Res Lett* 28(8):157–1510
- Otterå OH, Bentsen M, Drange H, Suo L (2010) External forcing as a metronome for Atlantic multidecadal variability. *Nature Geosci* 3(10):688–694
- Reverdin G, Niiler PP, Valdimarsson H (2003) North Atlantic Ocean surface currents. *J Geophys Res* 108(C1):3002. doi:[10.1029/2001JC001020](https://doi.org/10.1029/2001JC001020)
- Salas y Méliá D (2002) A global coupled sea ice–ocean model. *Ocean Model* 4:137–172
- Schlesinger ME, Ramankutty N (1994) An oscillation in the global climate system of period 65–70 years. *Nature* 367:723–726
- Stocker T (1998) The seesaw effect. *Science* 282:61–62
- Sutton R, Dong B (2012) Atlantic Ocean influence on a shift in European climate in the 1990s. *Nat Geo* 5:788–792. doi:[10.1038/ngeo1595](https://doi.org/10.1038/ngeo1595)
- Sutton RT, Hodson DLR (2005) Atlantic Ocean forcing of North American and European summer climate. *Science* 309:115–118
- Sutton RT, Norton WA, Jewson SP (2001) The North Atlantic Oscillation—what role for the ocean? *Atmos Sci Lett* 1:89–100
- Swingedouw D, Mignot J, Labetoulle S, Gilardi E, Madec G (2013) Initialization and predictability of the AMOC over the last 50 years in a climate model. *Clim Dyn* 40:23981–23990. doi:[10.1007/s00382-012-1516-8](https://doi.org/10.1007/s00382-012-1516-8)
- Taylor KE, Stouffer RJ, Meehl GA (2012) An overview of CMIP5 and the experiment design. *Bull Am Meteorol Soc* 93:485–498. doi:[10.1175/BAMS-D-11-00094.1](https://doi.org/10.1175/BAMS-D-11-00094.1)
- Terray L (2012) Evidence for multiple drivers of North Atlantic multi-decadal climate variability. *Geo Res Lett* 39:L19712. doi:[10.1029/2012GL053046](https://doi.org/10.1029/2012GL053046)
- Timmermann A, Latif M, Voss R, Groetzner A (1998) Northern Hemispheric interdecadal variability: a coupled air–sea mode. *J Clim* 11:1906–1931
- Ting M, Kushnir Y, Seager R, Li C (2009) Forced and internal twentieth-century SST in the North Atlantic. *J Clim* 22:1469–1881. doi:[10.1175/2008JCL12561.1](https://doi.org/10.1175/2008JCL12561.1)
- Torrence C, Compo GP (1998) A practical guide to wavelet analysis. *Bull Am Meteorol Soc* 79:61–78
- Trenberth KE, Shea DJ (2006) Atlantic hurricanes and natural variability in 2005. *Geophys Res Lett* 33:L12704. doi:[10.1029/2006GL026894](https://doi.org/10.1029/2006GL026894)
- Valcke S (2013) The OASIS3 coupler: a European climate modelling community software. *Geosci Model Dev* 6:373–388. doi:[10.5194/gmd-6-373-2013](https://doi.org/10.5194/gmd-6-373-2013)
- Vellinga M, Wu P (2004) Low-latitude fresh water influence on centennial variability of the thermohaline circulation. *J Clim* 17:4498–4511
- Vimont JV, Kossin JP (2007) The Atlantic Meridional mode and hurricane activity. *Geophys Res Lett* 34:L07709. doi:[10.1029/2007GL029683](https://doi.org/10.1029/2007GL029683)
- Wang C, Dong S, Evan AT, Foltz GR, Lee SK (2012) Multidecadal covariability of North Atlantic sea surface temperature, African dust, Sahel rainfall and Atlantic hurricanes. *J Clim* 25:5404–5415
- Willis JK (2010) Can in situ floats and satellite altimeters detect longterm changes in Atlantic Ocean overturning? *Geophys Res Lett* 37:L06602. doi:[10.1029/2010GL042372](https://doi.org/10.1029/2010GL042372)
- Wouters B, Drijfhout S, Halzeleger W (2012) Interdecadal North–Atlantic meridional overturning circulation variability in EC–EARTH. *Clim Dyn*. doi:[10.1007/s00382-012-1366-4](https://doi.org/10.1007/s00382-012-1366-4)
- Wunsch C (2002) What is the thermohaline circulation? *Science* 298:1179–1180
- Zhang R (2007) Anticorrelated multidecadal variations between surface and subsurface tropical North Atlantic. *Geophys Res Lett* 34:L12713. doi:[10.1029/2007GL030225](https://doi.org/10.1029/2007GL030225)
- Zhang R, Delworth TL (2005) Simulated tropical response to a substantial weakening of the Atlantic thermohaline circulation. *J Clim* 18:1853–1860
- Zhang Y, Wallace JM, Battisti DS (1997) ENSO-like interdecadal variability: 1900–93. *J Clim* 10:1004–1020